Mon. Not. R. Astron. Soc. **375,** 1381–1398 (2007) doi:10.1111/j.1365-2966.2006.11394.x

Kinematic structure in the Galactic halo at the North Galactic Pole: RR Lyrae and blue horizontal branch stars show different kinematics

T. D. Kinman,[1⋆] C. Cacciari,[2] A. Bragaglia,[2] A. Buzzoni[2] and A. Spagna[3]

[1]*NOAO, PO Box 26732, Tucson, AZ 85726-6732, USA*†
[2]*INAF, Osservatorio Astronomico di Bologna, Via Ranzani 1, I-40127 Bologna, Italy*
[3]*INAF, Osservatorio Astronomico di Torino, Via Osservatorio 20, I-10025 Pino Torinese, Italy*

Accepted 2006 December 11. Received 2006 November 28

ABSTRACT

Radial velocities and proper motions (derived from the GSC-II data base) are given for 38 RR Lyrae (RRL) stars and 79 blue horizontal branch (BHB) stars in a ∼200 deg^2 area around the North Galactic Pole (NGP). Both heliocentric (*UVW*) and galactocentric (V_R, V_ϕ, V_z) space motions are derived for these stars using a homogeneous distance scale consistent with $(m - M)_0 = 18.52$ for the Large Magellanic Cloud (LMC).

An analysis of the 26 RRL and 52 BHB stars whose height (Z) above the plane is less than 8 kpc shows that this halo sample is *not homogeneous*. Our BHB sample (like that of Sirko et al.) has a zero galactic rotation (V_ϕ) and roughly isotropic velocity dispersions. The RRL sample shows a definite retrograde rotation ($V_\phi = -95 \pm 29$ km s^{-1}) and non-isotropic velocity dispersions. The *combined* BHB and RRL sample has a retrograde galactic rotation (V) that is similar to that found by Majewski for his sample of subdwarfs in Selected Area (SA) 57. The velocity dispersion of the RRL stars that have a positive W motion is significantly smaller than the dispersion of those 'streaming down' with a negative W. Also, the ratio of RRL to BHB stars is smaller for the sample that has positive W.

Our halo sample occupies 10.4 kpc^3 at a mean height of 5 kpc above the Galactic plane. In this volume, one component (rich in RRL stars) shows retrograde rotation and the streaming motion that we associate with the accretion process. The other component (traced by the BHB stars) shows essentially no rotation and less evidence of streaming. These two components have horizontal branch (HB) morphologies that suggest that they may be the field star equivalents of the young and old halo globular clusters, respectively. Clearly, it is quite desirable to use more than one tracer in any kinematic analysis of the halo.

Key words: stars: horizontal branch – stars: kinematics – stars: variables: others – Galaxy: halo – Galaxy: structure.

1 INTRODUCTION

A well-known view about the globular-cluster halo is that it consists of an old halo and a young halo whose clusters have different horizontal branch (HB) morphologies that can be interpreted as an age difference (Zinn 1993). The two systems are to some extent coterminous but the clusters (whose $R_{\rm gal} < 6$ kpc) all belong to the old halo, while the young halo predominates in the outer parts of our Galaxy. Recent analyses of cluster ages (Rosenberg et al. 1999; De Angeli et al. 2005) show that the most metal-poor clusters are all older and coeval while the more metal-rich are younger and have a significant dispersion in age. The outer parts of the Galaxy show a somewhat larger dispersion in cluster age. The old halo system has a prograde galactic rotation while that of the young halo is retrograde. The old halo clusters have a high ratio of blue horizontal branch (BHB) to RR Lyrae (RRL) stars. Layden (1996) found that the field RRL stars with $3 \leqslant R_{\rm gal} \leqslant 6$ kpc were not kinematically as cool as the old halo clusters since they have a larger velocity dispersion and a milder prograde galactic rotation. Layden also analysed the radial velocities (RV) of the RRL stars with $|Z| > 5$ kpc and whose $R_{\rm gal}$ projected on the plane were between 6 and 10 kpc; these showed a marginally retrograde rotation. He accounted for these results in terms of the preferential destruction of the redder HB clusters in the inner halo and by these redder HB clusters having a greater fraction of RRL stars per unit luminosity. Borkova & Marsakov (2003) analysed the space motions of local RRL stars and also found evidence for two metal-poor ([Fe/H] < -1.0) systems. One (corresponding to the old

⋆E-mail: kinman@noao.edu
†NOAO is operated by AURA Inc. under contract with the National Science Foundation.

halo) is associated with blue-HB clusters and has a spherical distribution and a slightly prograde galactic rotation. The other (corresponding to the young halo) is more spatially extended, is associated with red HB clusters and has stars on eccentric and retrograde orbits. A correlation between the kinematics of globular clusters and their Oosterhoff type was pointed out by van den Bergh (1993) and also by Lee & Carney (1999). They found that Oosterhoff type II clusters belong to an older system with prograde orbits while Oosterhoff type I clusters belong to a younger (accreted) system on retrograde orbits. Lee & Carney associated the field RRL stars with $|Z| < 3$ kpc and $|Z| > 5$ kpc with Oosterhoff types II and I, respectively. The discovery of the disintegrating Sgr dwarf galaxy (Ibata, Gilmore & Irwin 1994) gave very strong support to the idea that the outer field star halo parallels the young cluster halo and is composed of the tidal debris from such accreted satellites. This has prompted searches for other satellites and consequent non-uniformities in the structure of the halo.

Surveys to discover such substructure include, among others, a K-giant survey (Morrison et al. 2000), an Automatic Plate Measuring Facility, Cambridge (APM) carbon star survey (Totten & Irwin 1998; Totten, Irwin & Whitelock 2000; Ibata et al. 2001) and the Sloan Digital Sky Survey (SDSS) for A stars (Yanny et al. 2000) and RRL stars (Ivezić et al. 2000). All have shown inhomogeneities in the distribution of stars in the outer halo that are mostly debris from the Sgr dSph (Newberg et al. 2002). More recent work with SDSS data has shown that these 'streams' and overdensities are very extensive (Lupton et al. 2005; Belokurov et al. 2006). Many of these surveys study the *distant* halo: 88 per cent of the large sample of BHB stars discovered by Sirko et al. (2004a) in the SDSS lie beyond 10 kpc and only four of these stars lie within 6 kpc. Thus, since proper motions are largely lacking for these stars, what we know of their kinematics can only come from analysing their RV (Sirko et al. 2004b; Thom et al. 2005).

The kinematics of the *local* halo are much better known because accurate proper motions are available (Martin & Morrison 1998; Maintz & de Boer 2005).[1] The mean halo rotation in the solar neighbourhood is close to zero (i.e. $\langle V \rangle \sim -220$ km s^{-1}) or is slightly prograde, and it is well established that the velocity dispersions in the local halo are non-isotropic ($\sigma_U > \sigma_V > \sigma_W$). Helmi et al. (1999) studied 97 metal-deficient ([Fe/H] $\leqslant -1.6$) red giants and RRL stars within 1 kpc of the Sun and found that about ∼10 per cent of these had space motions that showed that they came from a single disrupted satellite. This has been confirmed with a larger sample (234 stars within 2.5 kpc of the Sun) by Kepley et al. (2006) who also found evidence for two other possible 'streams'.

One of the first indications of structure in the halo was the discovery of retrograde motion for a group of subdwarf halo stars in Selected Area (SA) 57 at the North Galactic Pole (NGP) by Majewski (1992). Later, Majewski, Munn & Hawley (1996) (hereafter MMH) found that these halo stars were clumped in phase space and [Fe/H]; in particular, they found a retrograde group ($\langle V \rangle = -275 \pm 16$ km s^{-1}) with [Fe/H] < -0.8 moving towards the galactic plane. Kinman et al. (1996) also found a preponderance of negative RV (i.e. motion towards the plane) among BHB and RRL stars in the same area of the sky. A detailed analysis of the Sgr stream of debris using Two-Micron All-Sky Survey (2MASS) M-giants (Majewski et al. 2003; Law, Johnson & Majewski 2005) shows that the Sgr stream may be inflowing from the general direction of the NGP towards the solar neighbourhood. Martínez-Delgardo et al. (2006) have identified the Sgr leading arm with the overdensity in Virgo and predict highly negative RV in the North Galactic Cap but not at the area of the pole itself. On the other hand, neither Carney (1999) nor Chiba & Beers (2000) find retrograde motion among different samples of nearby halo stars whose $Z_{\max} \geqslant 4$ kpc. Vallenari et al. (2006) used the Padova Galaxy model to analyse the proper motions in a 26.7 deg^2 area near the NGP. Their halo component (for $Z < 7$ kpc) showed no significant rotation and had non-isotropic velocity dispersions. The colour distributions of their halo stars suggest that they are primarily redder [$(B - V) \geqslant +0.5$] giant stars. Other reports of nearby halo substructure include Chiba & Mizutani (2004), Altmann, Catelan & Zoccali (2005) and Meza et al. (2005) who discuss the debris from the globular-cluster ω Cen (probably the nucleus of a disrupted dwarf galaxy). The orbit discussed by Chiba & Mizutani does not rise more than 4 kpc above the plane in the direction of the NGP and so this debris is probably not connected with the substructure observed by MMH but might account for a halo overdensity of F and G stars observed by Gilmore, Wyse & Norris (2002). Duffau et al. (2006) have found a clump of both RRL and BHB stars at about 20 kpc that is coincident with an overdensity of F-type stars that were previously found by Newberg et al. (2002). Jurić et al. (2006) have found a significant overdensity of halo stars at 7 to 8 kpc in Virgo, although a search by Brown et al. (2004) for overdensities of BHB stars out to 9 kpc gave negative results. Clewley & Kinman (2006) have identified two new clumps that contain both RRL and BHB stars at distances of 8 and 9 kpc. There is therefore considerable evidence that structure exists in the nearby halo, but accurate proper motions and RV are needed in order to establish its significance.

This paper (a continuation of Kinman et al. 1996, 2003, 2005) derives space motions for 117 BHB and RRL stars in ∼200 deg^2 in the direction of the NGP. The sample of BHB stars in SA57 that comes from the Case Low-Dispersion Sky Survey (Sanduleak 1988), and was discussed by Kinman, Suntzeff & Kraft (1994), has been expanded to cover about six Palomar Schmidt Sky Survey fields (Fig. 1) using sources discussed in Section 2.1. The RRL stars in the same area of the sky have also been included and in many cases re-observed. A data base containing full details of these stars is in preparation (Kinman et al., in preparation). BHB and RRL stars continue to be recognized as prime halo tracers; recent surveys for

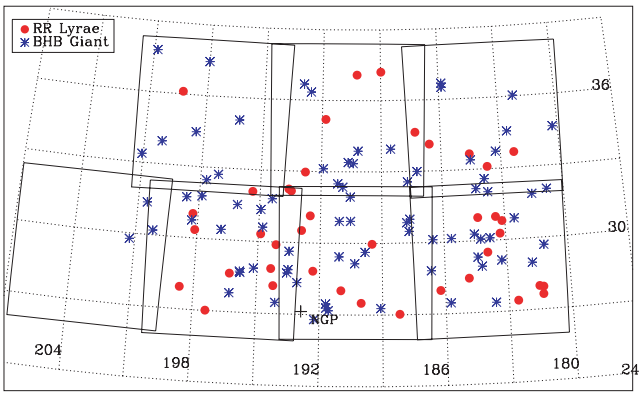

Figure 1. The POSS-I fields 266, 267, 268 (top) and 320, 321, 322 and 323 (bottom) used as first epoch plates to derive the proper motions of our target stars at the NGP. Right ascension, along the *x*-axis, is expressed in arc degrees. The cross shows the position of the NGP. For comparison, the J2000 coordinates of the SA57 are 13:08:38 +29:23:06 (197.158 +29.385 in decimal degrees).

[1] Summaries of other work on the local halo are given in Kinman et al. (2003) and in table 1 of Sirko et al. (2004b).

them include Sirko et al. (2004a), Vivas et al. (2001), Clewley et al. (2002, 2004, 2005), Brown et al. (2003, 2004, 2005) and Christlieb, Beers & Thom (2005). Red giants, subgiants and subdwarfs are more broadly representative of the halo but can be more difficult to separate from their disc counterparts, and estimates of their distances are commonly less exact than those of the HB stars. A major reason for studying the halo in the galactic polar regions is that the confusion between disc and halo stars is minimized in these directions; this is particularly important for the RRL stars which have a significant disc population. The galactic extinction is also minimal. Further, Kepley et al. (2006) have shown that streams may be more easily identified by their RV at the poles. Much previous work has depended on the analyses of RV alone. Surveys for distant halo stars tend to be made at high galactic latitudes well away from the apex and antapex of galactic rotation; the galactic rotation component of the RV is small compared with the random velocity components in these directions. Consequently, halo galactic rotations are not well determined from the RV alone. At the galactic poles, the relation between the galactic velocity vectors $\boldsymbol{U}$, $\boldsymbol{V}$ and $\boldsymbol{W}$ of a star and its distance, RV and proper motion is particularly simple. The $\boldsymbol{U}$ and $\boldsymbol{V}$ motions depend essentially only on the distance and proper motions while the $\boldsymbol{W}$ motion depends almost entirely on the RV. In principle therefore an analysis of the errors is more straightforward in the polar regions (and also along the prime galactic meridian) than in other directions.

It follows that it is important not only to get the best possible distances, RV and proper motions, but also to have a realistic assessment of their uncertainties. We feel that the proper motions that we have used (derived from the GSC-II data base) are the best currently available. We have estimated their errors from the proper motions of quasi-stellar objects (QSO) in the same fields. Presumably, the best proper motions will come from astrometric space missions such as *GAIA* and *Space Interferometry Mission* (*SIM*) (see e.g. *GAIA* Concept and Technology Study Report 2004, table A.4), but it will be several more years before these are available. The majority of our RV are of high quality ($\pm$10 km s^{-1}); there are some of lower accuracy but these do not significantly affect the conclusions of this study. Finally, the data base itself is not complete and it is hoped that it can be continually updated. In particular, it would be valuable to include the halo red giants in this region (Majewski, private communication). Clearly, this study is an ongoing project rather than one where definitive results can be obtained with the current data.

We present our sample of BHB and RRL stars and the data used for this study in Section 2; we discuss our analysis and results in Section 3 and Section 4 contains the summary and our conclusions.

2 THE DATA

2.1 Target selection

Our sample of halo tracers consists of 79 BHB and 38 RRL stars at distances between 1.5 and 16 kpc located in an area of approximately $22^\circ \times 12^\circ$ near the NGP. This area, shown in Fig. 1, is the combination of seven POSS-I fields where proper motions from the GSC-II data base were measured.

The BHB stars of our sample were selected from the surveys of Sanduleak (1988), Beers et al. (1996), MacConnell, Stephenson & Pesch (1993) and Kinman et al. (1994). They are listed in Table 1 with a simplified nomenclature: e.g. we use 16549-51 for BPS BS 16549-0051 (Beers et al. 1996), AF-003 for Case A-F 003 (Sanduleak 1988) and SA57-001 for SA57-001 (Kinman et al. 1994). The single ID used in Table 1 is that of the earliest of these catalogues in which the star is mentioned; alternative ID will be given in Kinman et al. (in preparation). These candidate BHB stars were confirmed by *uBV* photometry (Kinman et al. 1994) and spectroscopy. Most of the confirming spectra were taken at the Kitt Peak 4-m Mayall telescope (Kinman et al. 1996).

The RRL stars (Table 2) were mostly taken from the General Catalogue of Variable Stars (GCVS; Kholopov 1985) and subsequent name lists, and have the traditional identification by constellation; those without GCVS names are taken from Kinman (2002). These are NSV5476, AF-791, AF-155, SA57-19, SA57-47, SA57-60 and AF-882. The data for AF-031 and AF-042 are as yet unpublished.

Intensity-weighted mean V magnitudes of the RRL stars are derived from recently observed light curves. Spectra of several RRL stars were obtained at the 3.5-m Telescopio Nazionale Galileo (TNG). Only six of these RRL stars and none of the BHB stars in our current sample are included in the catalogue of halo stars by Beers et al. (2000).

K magnitudes are available in the 2MASS catalogue for all our BHB and RRL stars. The data from which the kinematic properties of these stars were derived are given for the BHB and RRL stars in Tables 1 and 2, respectively. More detailed descriptions of this photometric and spectroscopic data will be given in Kinman et al. (in preparation).

2.2 Reddenings, absolute magnitudes and distances

2.2.1 Reddenings

The reddening $E(B-V)$ was taken from Schlegel, Finkbeiner & Davis (1998). The reddening corrections for other colours are derived from the relations $E(V-K) = 2.75E\ (B-V), A_V = 3.1E(B-V)$ and $A_K = 0.35E(B-V)$ (Cardelli, Clayton & Mathis 1989).

2.2.2 Absolute magnitudes and distances: RRL stars

We consider three ways to estimate the absolute magnitudes and hence parallaxes of our RRL stars:

(i) The visual absolute magnitude M_V is given in terms of the metallicity [Fe/H] by the empirical relation:

$$M_V = 0.214[\mathrm{Fe/H}] + 0.86. \quad (1)$$

We adopt the coefficients given by Clementini et al. (2003) which imply that $M_V = 0.54$ for $[\mathrm{Fe/H}] = -1.5$. They give a LMC modulus of $\sim$18.52 using the $\langle V_0 \rangle = 19.064$ that Clementini et al. (2003) derive from their sample of about 100 RRL stars in the LMC bar. This M_V estimate is therefore squarely in the middle of the range derived from recent LMC distance determinations, most notably 18.50 (Freedman et al. 2001) and 18.54 (Tammann, Sandage & Reindl 2003). The metallicity, [Fe/H], however, is known for only just over half of our RRL sample (see Table 2). We assume $[\mathrm{Fe/H}] = -1.6$ for the remaining stars since this is close to the mean metallicity of a halo population. An error of $\pm$0.5 dex in [Fe/H] leads to an error of $\pm$0.1 mag in the distance modulus and about 5 per cent in the parallax. The parallaxes derived by this method (Π_V) and their errors (σ_Π) are given in Columns 8 and 9, respectively, in Table 2.

(ii) The infrared absolute magnitude M_K is derived from the metallicity and period. In the case of the type *ab* RRL stars, we use the relation in the form given by Nemec, Linnell-Nemec & Lutz (1994):

$$M_K = -2.40 \log P + 0.06[\mathrm{Fe/H}] - 1.06 \quad (2)$$

where the zero point is on the same scale as that given in (iii) below. In the case of the c-type variables (indicated by an asterisk against

Table 1. The BHB stars of our sample. The coordinates are for J2000. The parallaxes Π_{HBP}, Π_{HBC} and Π_{HBK} are defined in Section 2.2.3; the error σ_Π refers to the adopted parallax Π_{HBP}. Proper motions and their errors (Columns 12–15) are in mas yr^{-1}. RV and their errors (Columns 16 and 17) are in km s^{-1}.

ID	RA	Dec.	V	$B-V$	$E(B-V)$	K	Π_{HBP}	σ_Π	Π_{HBC}	Π_{HVK}	μ_α	$\sigma\ \mu_\alpha$	μ_δ	$\sigma\ \mu_\delta$	RV	σRV
(1)	(2)	(3)	(4)	(5)	(6)	(7)	(8)	(9)	(10)	(11)	(12)	(13)	(14)	(15)	(16)	(17)
16549-51	12 01 02.4	34 37 40	13.67	0.078	0.016	13.30 A	0.271	0.014	0.280	0.258	−15.8	1.9	−7.9	1.1	46	50
AF-003	12 03 20.1	32 01 38	16.48	0.230	0.019	15.35 C	0.066	0.003	0.067	0.067	1.0	4.1	−3.8	4.6	−75	40
AF-006	12 04 43.1	29 41 50	13.64	0.007	0.016	13.54 A	0.309	0.026	0.332	0.282	−9.2	3.5	−20.0	1.5	28	10
AF-011	12 06 19.5	31 51 37	15.85	0.101	0.019	14.72 U	0.098	0.004	0.100	0.090	2.4	3.4	−13.7	6.2	−92	10
AF-013	12 07 11.2	28 58 52	16.78	0.115	0.019	17.18 U	0.063	0.003	0.064	0.086	−3.8	2.2	−4.0	1.5	128	40
AF-727	12 08 42.0	36 02 08	13.93	0.137	0.019	13.52 A	0.229	0.009	0.231	0.228	1.4	1.6	−2.0	1.8	−24	10
AF-022	12 10 08.2	30 53 00	16.37	0.082	0.019	15.96 U	0.078	0.004	0.081	0.074	−1.9	2.1	−5.9	1.0	−40	10
AF-729	12 10 26.4	34 32 54	15.24	0.146	0.013	14.70 A	0.123	0.005	0.123	0.121	−3.6	1.9	−7.8	1.9	−32	40
AF-029	12 12 59.8	33 43 13	14.85	0.131	0.013	14.22 A	0.148	0.006	0.150	0.144	0.4	2.8	−3.9	1.7	−62	10
AF-030	12 13 01.9	29 09 05	14.85	0.044	0.023	14.48 A	0.169	0.012	0.178	0.152	−7.8	2.4	−8.9	1.8	42	10
16022-26	12 14 29.2	27 23 52	14.65	0.097	0.023	14.18 A	0.172	0.008	0.177	0.164	−4.8	1.6	−9.4	2.5	−29	50
AF-038	12 15 01.6	32 02 21	15.63	0.049	0.016	15.23 B	0.114	0.007	0.120	0.104	−6.8	1.7	−7.9	3.3	−78	10
AF-039	12 15 04.8	30 06 18	16.65	−0.006	0.019	15.66 D	0.081	0.007	0.087	0.062	−5.9	1.5	−1.0	1.6	58	40
AF-041	12 15 35.4	32 35 38	15.02	0.168	0.013	14.26 A	0.134	0.005	0.134	0.132	−9.2	1.6	−9.0	1.9	95	10
AF-045	12 16 49.9	28 56 06	13.45	0.129	0.026	12.86 A	0.292	0.012	0.296	0.281	−4.9	1.2	−2.0	1.3	17	10
AF-046	12 16 53.7	30 04 09	15.98	0.130	0.023	15.69 D	0.090	0.004	0.091	0.092	−3.9	1.6	−2.0	3.4	64	10
AF-048	12 17 20.9	32 11 27	13.92	−0.008	0.013	13.85 A	0.278	0.025	0.301	0.248	−7.8	2.1	−9.9	1.8	22	10
AF-050	12 17 34.8	29 19 24	16.57	0.222	0.026	15.89 U	0.065	0.003	0.065	0.066	−2.0	3.2	−4.9	2.2	27	40
AF-052	12 18 05.5	30 17 25	14.74	0.081	0.019	14.30 A	0.166	0.009	0.172	0.157	−8.9	4.2	−6.9	2.7	−66	10
AF-053	12 18 08.5	33 24 37	15.19	0.026	0.013	15.09 B	0.144	0.011	0.153	0.137	−1.8	1.3	−13.0	2.9	11	10
AF-063	12 22 34.2	30 08 36	16.29	0.092	0.019	16.19 U	0.080	0.004	0.083	0.083	−4.0	1.8	−3.9	1.0	−103	10
16026-28	12 23 02.6	27 27 16	13.65	0.009	0.019	13.50 A	0.310	0.026	0.333	0.278	−0.5	1.7	−4.2	1.3	−85	10
AF-754	12 23 24.9	36 31 09	15.25	0.106	0.013	14.84 A	0.126	0.005	0.128	0.123	−3.0	1.3	−6.0	3.6	−15	40
AF-755	12 23 26.9	36 41 12	15.46	0.034	0.013	15.06 B	0.126	0.009	0.133	0.112	−4.9	2.5	−6.0	3.1	−120	40
AF-068	12 26 10.3	30 07 13	14.63	0.108	0.019	14.12 A	0.170	0.008	0.173	0.163	−4.0	2.6	−5.8	1.5	−134	10
AF-070	12 26 37.4	28 49 24	15.19	0.047	0.023	14.98 B	0.144	0.010	0.151	0.135	−5.5	1.4	−4.8	2.1	181	10
AF-073	12 28 56.2	32 59 29	16.81	0.158	0.016	15.98 D	0.059	0.002	0.060	0.058	1.0	1.6	−4.0	1.5	−41	40
AF-075	12 30 33.4	30 59 59	15.36	0.115	0.016	14.89 A	0.120	0.005	0.122	0.116	0.3	2.8	−10.9	2.0	−50	10
AF-076	12 30 44.4	30 29 29	15.72	0.128	0.019	15.03 B	0.101	0.004	0.102	0.097	−1.8	2.5	−6.0	0.7	37	10
AF-077	12 30 51.9	32 34 07	15.60	0.102	0.013	15.10 B	0.108	0.005	0.110	0.103	−0.6	3.1	−8.2	4.0	−159	10
AF-078	12 31 10.6	30 51 26	14.05	0.092	0.016	13.51 A	0.224	0.011	0.230	0.211	2.1	0.9	−5.9	2.0	−178	10
AF-769	12 34 07.2	33 57 01	13.66	0.062	0.019	13.32 A	0.281	0.017	0.293	0.262	−17.8	2.0	−16.6	2.5	9	10
16026-67	12 36 21.8	27 16 34	13.40	0.006	0.019	13.28 A	0.350	0.030	0.377	0.314	−15.7	2.3	−19.8	3.8	−29	10
AF-100	12 39 18.2	29 37 53	13.74	0.090	0.013	13.35 A	0.257	0.012	0.263	0.247	−16.9	1.5	−9.1	2.2	57	10
16466-08	12 40 41.7	33 52 27	15.22	−0.014	0.016	15.09 C	0.157	0.015	0.170	0.135	−7.9	2.8	−5.2	1.4	17	40
AF-108	12 41 17.6	29 09 15	13.86	0.035	0.013	13.67 A	0.262	0.018	0.277	0.245	−17.9	1.8	−20.9	1.8	−70	10
AF-111	12 41 38.4	33 20 55	14.33	0.087	0.016	14.08 A	0.198	0.010	0.203	0.195	−12.0	1.9	3.2	1.9	−18	10
AF-112	12 42 07.9	30 55 41	13.21	0.006	0.016	13.09 A	0.378	0.032	0.406	0.340	1.0	1.9	−9.0	1.6	2	10
AF-113	12 42 12.4	31 56 48	11.78	0.139	0.016	11.22 A	0.611	0.025	0.614	0.598	−25.9	1.9	−35.8	1.7	4	10
AF-115	12 42 39.3	33 23 52	15.42	0.068	0.016	15.02 B	0.123	0.007	0.127	0.115	−5.8	1.7	−8.6	1.2	13	10
16466-15	12 43 41.8	32 21 28	13.14	0.089	0.013	12.71 A	0.339	0.016	0.348	0.324	−5.9	2.5	−3.8	4.1	145	10
AF-130	12 44 18.6	29 26 20	15.92	0.180	0.013	15.25 B	0.088	0.004	0.088	0.087	−1.0	1.9	−4.0	0.9	106	10
AF-131	12 44 18.6	30 55 22	15.58	0.119	0.016	15.01 B	0.108	0.005	0.109	0.104	−4.0	1.9	−6.0	1.7	47	10
AF-134	12 44 42.2	32 29 55	12.76	0.170	0.013	12.04 A	0.378	0.015	0.378	0.373	6.2	1.9	−23.1	1.1	−27	10

Table 1 – *continued*

ID (1)	RA (2)	Dec. (3)	V (4)	$B-V$ (5)	$E(B-V)$ (6)	K (7)	$\Pi_{\rm HBP}$ (8)	σ_Π (9)	$\Pi_{\rm HBC}$ (10)	$\Pi_{\rm HVK}$ (11)	μ_α (12)	$\sigma\ \mu_\alpha$ (13)	μ_δ (14)	$\sigma\ \mu_\delta$ (15)	RV (16)	σRV (17)
16031-44	12 46 15.6	27 10 47	13.80	0.145	0.013	13.23 A	0.238	0.010	0.239	0.234	1.4	1.2	−13.0	3.2	11	10
15622-48	12 46 43.7	27 17 17	14.47	0.153	0.013	13.97 A	0.174	0.007	0.174	0.174	−3.1	1.4	−10.2	2.6	−69	10
15622-07	12 46 47.3	27 27 44	12.86	0.121	0.013	12.44 A	0.374	0.016	0.378	0.369	−5.1	2.3	−12.9	3.3	−37	10
AF-138	12 47 37.2	33 07 28	14.72	−0.009	0.013	14.65 A	0.193	0.017	0.209	0.171	−8.9	3.0	−10.5	1.6	101	10
15622-09	12 48 58.8	26 48 04	13.08	0.122	0.010	12.48 A	0.336	0.014	0.339	0.324	−1.7	1.4	−14.0	2.5	−121	10
AF-797	12 50 23.2	36 20 53	15.42	0.074	0.016	15.07 A	0.122	0.006	0.126	0.116	−8.0	2.2	−6.0	0.3	85	40
AF-804	12 51 52.7	36 40 42	14.07	0.098	0.016	13.64 A	0.221	0.010	0.225	0.212	−13.0	2.3	−5.9	1.0	94	10
SA57-001	12 52 18.7	28 19 58	14.43	0.155	0.010	13.76 A	0.176	0.007	0.176	0.173	−1.9	2.8	−18.4	1.8	−124	10
SA57-006	12 53 57.3	29 38 08	13.99	0.083	0.010	13.58 A	0.229	0.011	0.235	0.218	−14.6	2.7	−5.6	2.2	112	10
SA57-007	12 54 03.7	28 51 47	12.18	−0.010	0.013	12.11 A	0.626	0.058	0.678	0.553	−13.9	1.6	−28.5	2.2	−92	50
SA57-009	12 54 18.0	28 43 42	15.96	0.204	0.013	15.14 B	0.085	0.003	0.085	0.085	−9.6	2.7	−9.1	1.7	47	10
SA57-017	12 56 23.8	27 28 39	13.41	0.084	0.016	13.00 A	0.304	0.015	0.313	0.289	−25.4	4.7	−10.6	3.5	−4	10
SA57-021	12 57 34.6	31 48 45	16.62	−0.066	0.016	16.43 U	0.097	0.011	0.107	0.069	−6.0	2.2	5.8	3.3	−70	40
SA57-029	12 59 13.6	30 36 19	16.31	0.085	0.010	15.72 D	0.079	0.004	0.081	0.073	−2.9	1.6	−4.0	1.8	−182	40
SA57-032	12 59 43.3	31 20 30	15.13	0.155	0.013	14.63 A	0.128	0.005	0.128	0.128	−7.8	1.5	−8.0	2.5	−14	10
SA57-036	13 00 41.2	28 52 37	16.23	0.062	0.010	15.37 B	0.084	0.005	0.087	0.075	−3.9	1.9	−5.9	2.7	−5	10
SA57-040	13 03 13.6	28 40 11	15.14	0.080	0.010	14.67 A	0.135	0.007	0.139	0.127	−2.9	1.5	−2.5	1.2	30	10
SA57-041	13 03 20.6	28 43 28	16.33	0.092	0.010	15.62 C	0.077	0.004	0.079	0.072	−4.9	1.9	−3.5	1.8	127	10
SA57-045	13 04 22.7	31 30 25	15.31	0.108	0.010	15.12 B	0.122	0.005	0.123	0.125	1.0	1.4	−7.9	1.0	−135	10
AF-825	13.04 56.3	35 03 31	14.32	0.051	0.013	14.08 A	0.207	0.013	0.216	0.196	−5.9	0.8	−5.1	1.4	−139	50
SA57-046	13 05 08.7	27 48 01	16.71	0.148	0.013	16.76 U	0.062	0.002	0.062	0.072	−4.9	1.7	−4.4	2.2	151	40
SA57-055	13 07 19.4	30 25 56	16.03	0.140	0.013	15.58 C	0.086	0.003	0.086	0.085	−1.0	3.1	−5.9	0.7	−224	10
AF-841	13 08 30.3	32 43 40	14.06	0.091	0.013	13.62 A	0.222	0.010	0.227	0.212	−7.8	1.2	−10.1	1.7	−25	10
AF-848	13 10 48.5	32 28 19	11.75	0.001	0.010	11.64 A	0.732	0.061	0.786	0.661	−9.8	3.0	−18.0	2.8	−116	10
SA57-066	13 11 29.4	31 47 06	14.68	0.116	0.013	14.08 A	0.163	0.007	0.165	0.156	−3.0	3.4	−3.9	2.1	−243	10
AF-854	13 12 01.6	37 26 55	15.11	0.058	0.013	14.77 A	0.142	0.008	0.148	0.133	−10.9	1.8	−0.0	1.4	−10	50
SA57-080	13 13 10.2	30 45 00	14.16	0.077	0.013	13.90 A	0.215	0.011	0.222	0.210	−8.0	1.2	−4.8	2.5	−46	10
AF-866	13 13 39.3	34 27 18	13.93	0.059	0.010	13.64 A	0.243	0.014	0.252	0.230	−6.0	1.8	−11.0	2.8	−41	50
SA57-087	13 14 29.3	31 42 15	15.97	0.093	0.010	15.45 C	0.091	0.004	0.093	0.086	−4.5	2.6	−3.8	2.6	−112	10
AF-900	13 20 25.1	33 57 56	13.71	0.013	0.013	13.55 A	0.293	0.023	0.313	0.265	−9.6	1.5	−10.8	0.6	92	50
SA57-111	13 20 37.2	30 12 14	16.47	0.094	0.016	15.66 U	0.073	0.003	0.075	0.068	−5.9	1.3	−4.0	1.5	−138	10
AF-909	13 22 12.0	31 21 31	15.26	0.023	0.013	15.09 A	0.141	0.010	0.149	0.130	−1.9	1.3	−5.9	1.2	−144	10
AF-914	13 23 21.0	37 47 05	12.27	−0.003	0.010	12.16 A	0.581	0.050	0.626	0.519	−36.2	3.4	−15.0	3.4	95	50
AF-916	13 24 15.4	33 22 13	14.00	0.181	0.010	13.69 A	0.210	0.008	0.211	0.222	−0.2	1.3	−6.0	1.7	−132	50
AF-918	13 25 02.6	29 46 18	14.08	0.028	0.013	13.87 A	0.240	0.017	0.254	0.220	−7.9	2.3	−5.9	1.6	−24	50

Table 2. The RRL stars of our sample. $\langle K\rangle$ magnitudes are corrected for phase effect as described in the text. The parallaxes labelled Π_V, Π_K and $\Pi_{\rm HB}$ were estimated as described in Section 2.2.2. The error $\sigma\,\Pi$ refers to the adopted parallax Π_V. RV and σRV are in km s^{-1}.

ID (1)	RA (2)	Dec. (3)	logP (4)	[Fe/H] (5)	$\langle V\rangle$ (6)	$\langle K\rangle$ (7)	$E(B-V)$ (8)	Π_V (9)	$\sigma\,\Pi$ (10)	Π_K (11)	$\Pi_{\rm HB}$ (12)	μ_α (13)	$\sigma\ \mu_\alpha$ (14)	μ_δ (15)	$\sigma\ \mu_\delta$ (16)	RV (17)	σRV (18)
GR-Com	12 05 18.6	27 56 58	−0.282	–	16.33	15.14 B	0.021	0.071	0.004	0.075	0.072	−3.8	1.3	−6.0	1.7	–	–
GH-Com	12 05 24.5	27 38 22	−0.352	–	15.38	14.42 A	0.020	0.110	0.007	0.114	0.112	−1.7	1.5	−8.9	2.3	–	–
IQ-Com	12 06 03.6	27 59 18	−0.294	–	15.70	14.68 A	0.020	0.095	0.006	0.095	0.095	−3.9	1.8	−1.1	1.1	–	–
NSV5476	12 09 17.0	33 39 36	−0.486∗	–	14.96	14.16 A	0.013	0.132	0.008	0.128	0.135	−4.1	1.9	−8.3	1.1	−27	50
V-Com	12 10 15.9	27 25 54	−0.329	−1.80	13.25	12.39 A	0.022	0.289	0.009	0.280	0.296	−15.7	1.9	−0.8	10.6	+23	28
CD-Com	12 12 34.0	30 48 03	−0.229	−1.94	15.40	14.12 A	0.018	0.105	0.004	0.105	0.113	−12.7	1.4	−11.0	1.9	−203	10
AF-031	12 13 04.4	30 16 38	−0.519∗	–	15.49	14.74 A	0.019	0.104	0.006	0.103	0.107	−7.8	0.8	−7.0	3.0	−167	50
TU-Com	12 13 46.9	30 59 08	−0.336	−1.59	13.80	13.08 A	0.018	0.227	0.007	0.206	0.233	−0.8	1.9	−19.7	9.1	−98	10
CK-Com	12 14 50.6	33 06 07	−0.159	−1.85	14.62	13.50 A	0.012	0.150	0.008	0.139	0.153	−7.4	1.4	−16.0	1.2	−88	10
AF-042	12 15 39.3	29 30 43	−0.502∗	–	16.35	15.31 U	0.021	0.070	0.004	0.074	0.072	−3.9	2.3	−4.0	2.0	–	–
CL-Com	12 17 16.3	30 58 39	−0.255	−1.17	15.10	13.79 A	0.016	0.129	0.005	0.138	0.131	−1.0	2.6	−5.9	0.6	−34	10
AT-CVn	12 18 17.1	33 39 56	−0.446∗	–	14.76	13.76 A	0.013	0.144	0.009	0.148	0.147	−5.9	2.1	−6.1	4.0	+94	50
GY-Com	12 19 26.0	28 27 28	−0.272	–	15.89	14.58 A	0.026	0.087	0.006	0.097	0.089	+2.9	1.5	−5.9	1.8	–	–
GS-Com	12 24 56.1	27 59 08	−0.276	–	16.44	15.04 A	0.021	0.067	0.004	0.078	0.069	−1.0	1.4	−4.9	4.7	–	–
RR-CVn	12 29 07.6	34 38 51	−0.253	−1.50	12.72	11.61 A	0.016	0.375	0.014	0.372	0.381	−19.1	2.2	−24.7	3.2	−5	10
S-Com	12 32 45.7	27 01 46	−0.232	−1.79	11.64	10.60 A	0.019	0.589	0.014	0.571	0.604	−19.6	4.4	−18.4	3.9	−55	4
SV-CVn	12 35 56.0	37 12 26	−0.175	−2.20	12.65	11.46 A	0.018	0.362	0.015	0.358	0.373	−6.6	0.9	−25.7	2.2	+29	28
FV-Com	12 37 57.2	29 58 06	−0.326	–	14.65	13.46 A	0.018	0.153	0.010	0.171	0.156	+2.1	1.9	−7.0	2.0	−186	50
U-Com	12 40 03.4	27 29 57	−0.534∗	−1.25	11.73	10.94 A	0.016	0.602	0.014	0.603	0.614	−49.7	2.7	−16.4	2.1	−22	3
SW-CVn	12 40 55.1	37 05 07	−0.355	−1.53	12.84	11.98 A	0.013	0.352	0.015	0.351	0.359	−17.8	2.7	−6.4	2.6	−18	21
DV-Com	12 43 54.4	28 01 16	−0.267	−1.74	14.84	13.63 A	0.014	0.137	0.003	0.148	0.140	+1.9	1.4	−12.0	2.8	−136	10
AF-791	12 47 16.3	35 12 06	−0.209	−1.68	14.77	13.55 A	0.015	0.144	0.009	0.144	0.147	−10.0	1.8	+5.9	1.6	−200	10
AW-Com	12 49 18.0	28 49 27	−0.347	–	15.64	14.87 B	0.015	0.095	0.006	0.092	0.098	+2.4	1.0	−5.0	2.1	–	–
TX-Com	12 50 00.7	31 08 25	−0.270	–	14.29	13.25 A	0.012	0.179	0.011	0.177	0.182	+0.2	2.1	−15.9	1.4	−118	50
AP-CVn	12 51 10.6	32 58 19	−0.241	–	13.90	12.70 A	0.013	0.215	0.014	0.221	0.219	−13.0	1.5	−4.9	2.0	−20	50
EM-Com	12 51 38.3	30 31 04	−0.266	−1.80	15.41	14.26 A	0.014	0.105	0.004	0.110	0.107	−1.2	2.5	−7.9	1.6	−127	10
AF-155	12 53 51.2	32 09 56	−0.526∗	−1.56	15.05	14.22 A	0.014	0.127	0.008	0.131	0.129	−3.4	2.1	−5.9	2.5	−119	32
TY-CVn	12 54 21.6	32 14 34	−0.290	−1.23	13.60	12.65 A	0.015	0.247	0.016	0.239	0.252	−24.4	1.6	−3.3	3.3	+74	16
IP-Com	12 56 30.8	29 53 36	−0.193	−1.48	14.85	13.49 A	0.012	0.138	0.009	0.146	0.141	−3.7	2.3	−13.8	3.0	−137	30
SA57-19	12 56 51.2	28 10 35	−0.588∗	–	14.58	13.88 A	0.010	0.156	0.009	0.164	0.161	−9.7	1.6	−8.0	1.6	+49	50
EO-Com	12 57 22.1	28 53 20	−0.199	−1.67	14.74	13.56 A	0.011	0.144	0.005	0.142	0.147	−11.7	2.7	−9.1	1.4	+72	10
UV-Com	12 59 34.1	30 19 25	−0.211	−1.61	15.58	14.31 A	0.011	0.099	0.003	0.102	0.101	−8.8	1.0	−2.1	2.0	+58	10
TZ-CVn	13 01 29.2	32 05 13	−0.258	–	14.17	13.32 A	0.012	0.189	0.012	0.170	0.193	−2.4	3.1	−15.1	2.7	−167	50
SA57-47	13 05 14.5	28 37 14	−0.188	−1.51	14.43	13.16 A	0.011	0.168	0.010	0.169	0.171	−9.8	1.9	−23.1	1.9	−166	37
SA57-60	13 09 29.7	27 01 00	−0.206	–	14.23	12.88 A	0.017	0.185	0.011	0.196	0.189	−11.0	2.1	−14.7	2.6	−109	50
EW-Com	13 13 01.7	31 01 22	−0.274	−1.92	15.02	14.26 A	0.012	0.124	0.003	0.111	0.128	−8.4	1.3	−1.8	2.2	+19	10
IS-Com	13 14 38.8	27 56 30	−0.502∗	–	13.80	12.96 A	0.013	0.225	0.014	0.228	0.230	−13.4	1.4	−15.6	1.8	−163	10
AF-882	13 17 03.5	36 06 58	−0.169	–	14.60	13.50 A	0.011	0.155	0.009	0.142	0.158	−4.1	1.5	−7.9	1.6	−123	50

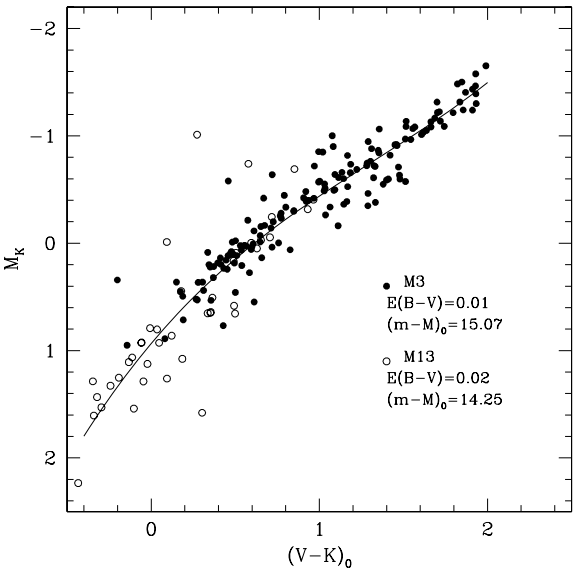

Figure 2. The combined HB of the globular clusters M3 and M13 in the infrared (IR) plane M_K versus $(V-K)_0$ (data from Valenti et al. 2004). The data have been corrected for reddening and shifted according to the individual distance moduli, as specified. The line shows the relation in equation (3).

their log P in Column 4 of Table 2), the periods must be 'fundamentalized' before using them in this relation. For this, we have assumed that the ratio of the first overtone (c-type) to fundamental (*ab*-type) period is 0.745 (Clement et al. 2001). The parallaxes derived in this way (Π_K) are given in Column 11 of Table 2.

(iii) The infrared absolute magnitude M_K is derived from the $(V-K)_0$ colour using an empirical relation derived from data for non-variable stars in the globular clusters M3 and M13 (Valenti et al. 2004). These two clusters have similar metallicities which are both close to the mean for the field halo population. We assumed reddenings $E(B-V)$ of 0.01 and 0.02 and distance moduli $(m-M)_0$ of 15.07 and 14.25 for M3 and M13, respectively. These M3 and M13 data (Fig. 2) can be fitted by the 3σ rejection cubic polynomial:

$$M_K = 0.878 - 1.812(V-K)_0 + 0.675(V-K)_0^2 - 0.183(V-K)_0^3. \quad (3)$$

This relation only holds for stars with the metallicity of M3 and M13. The M_K versus $(V-K)_0$ relations for zero age horizontal branch (ZAHB) stars of different [Fe/H] were obtained from the models of Vandenberg et al. (2000). These models were kindly transformed into M_K versus $(V-K)_0$ by A. Sollima using the colour–temperature relation given by Bessell, Castelli & Plez (1998). The ZAHB relations show that in the colour range of the RRL stars an expression for M_K needs a metallicity term $\sim +0.18$[Fe/H]. Equation (3) is therefore amended to

$$M_K = 1.166 + 0.18[\mathrm{Fe/H}] - 1.812(V-K)_0 + 0.675(V-K)_0^2 - 0.183(V-K)_0^3. \quad (4)$$

The parallaxes (Π_{HB}), derived from equation (4), are given in Column 12 of Table 2.

The mean difference between the M_K derived from equation (4) and that from equation (2) for our 38 RRL stars is $+0.025 \pm 0.022$ mag with a dispersion of 0.134 mag; this is satisfactorily small. Mean infrared magnitudes $\langle K\rangle$ were derived from the single epoch 2MASS magnitudes using the template K light curves given by Jones, Carney & Fulbright (1996) and the most appropriate ephemerides available. The K amplitudes are such that errors of $\sim$0.20 mag in $\langle K\rangle$ are possible if the estimated phases are in error by 0.1. The letter following $\langle K\rangle$ in Table 2 gives the photometric quality[2] of the 2MASS data. 35 of the RRL sample have quality A ($\sigma_K \leqslant 0.10$ mag); for these $\Pi_K/\Pi_V = 1.010 \pm 0.010$ with a dispersion of 0.062. The 20 with no metallicity estimate (for which we assumed [Fe/H] $= -1.6$) have $\Pi_K/\Pi_V = 1.022 \pm 0.014$ and a dispersion of 0.064 while for the 15 variables for which [Fe/H] is known, this ratio is 0.996 ± 0.015 with a dispersion of 0.058. The parallaxes derived from infrared magnitudes provide a useful confirmation of the validity of the parallax (Π_V) derived from visual magnitudes, but the greater uncertainty in the infrared magnitudes compared with the visual magnitudes of our program stars and the greater uncertainties of equations (2), (3) and (4) compared with equation (1) has led us to adopt (Π_V) alone for the calculation of the RRL distances.

2.2.3 *Absolute magnitudes and distances: BHB stars*

For the BHB stars, M_V can be estimated from the M_V versus $(B-V)$ relation given by Preston, Shectman & Beers (1991). We adjusted this relation so as to be consistent with the absolute scale that we have adopted for the RRL stars to get

$$M_V = 1.00 - 4.423(B-V)_0 + 17.74(B-V)_0^2 - 35.73(B-V)_0^3. \quad (5)$$

The parallax derived from equation (5) is given as Π_{HBP} in Table 1. Various problems involved with deriving M_V from $(B-V)_0$ have been discussed by Brown et al. (2005). One concern is that the data for the 15 globular clusters on which this relation is based are now quite old. For comparison, we therefore derived a similar cubic from more recent data for the intermediate-metallicity clusters M3 (Ferraro et al. 1997) and M13 (Paltrinieri et al. 1998):

$$M_V = 1.145 - 5.615(B-V)_0 + 16.28(B-V)_0^2 - 14.93(B-V)_0^3. \quad (6)$$

The parallax derived from equation (6) is given as Π_{HBC} in Table 1. The mean value of the ratio $\Pi_{\mathrm{HBC}}/\Pi_{\mathrm{HBP}}$ is 1.032 ± 0.003 with a dispersion of 0.027. This ratio is adjusted to be unity at the blue edge of the instability strip[3] and increases to 1.107 for the bluest BHB star in our sample [$(B-V)_0 = -0.08$]. We assume that the difference (Δ) between these parallaxes is a measure of the likely systematic error in Π_{HBP}. If σ is the error in Π_{HBP} [as deduced from the error in $(B-V)_0$] then its adopted error (σ_Π given in Column 9 of Table 1) is $\sqrt{(\Delta^2+\sigma^2)}$.

Equation (3) can also be used to derive a parallax for the BHB stars (Π_{HVK} in Column 10 of Table 1). 50 of them have 2MASS K magnitudes of quality A; for these the ratio $\Pi_{\mathrm{HVK}}/\Pi_{\mathrm{HBP}} = 0.950 \pm 0.005$ with a dispersion of 0.036. This ratio (adjusted to be unity at the blue edge of the instability strip) decreases to 0.888 for the bluest star in this sample [$(B-V)_0 = -0.02$]. Equation (3) is least defined for its bluest colours since these correspond to the faintest HB stars in the calibrating globular clusters. The derivation of parallaxes from $(V-K)_0$ for these stars is likely to have significant advantages over the use of $(B-V)_0$, but currently we need better calibration and more accurate magnitudes for the fainter program stars before the

[2] The letters A, B, C, D and U correspond to the observation having a signal-to-noise ratio (S/N) of >10, >7, >5, <5 and being an upper limit, respectively.

[3] $(B-V)_0 \sim 0.20$ (Sandage 2006, Fig. 8).

Table 3. Mean galactocentric radial velocities $\langle RV_{gal} \rangle$ for our sample of NGP halo stars at different heights (Z) above the plane and RA.

Z (kpc)	RA (h:m)	N	$\langle RV_{gal} \rangle$ (km s^{-1})	Dispersion (km s^{-1})
<4	All	26	$+9.6 \pm 14.1$	66.8 ± 9.3
>4	All	84	-26.1 ± 10.7	92.0 ± 7.1
>4	<13:00	61	-17.4 ± 12.3	91.7 ± 8.3
>4	>13:00	23	-48.9 ± 21.2	94.1 ± 13.9

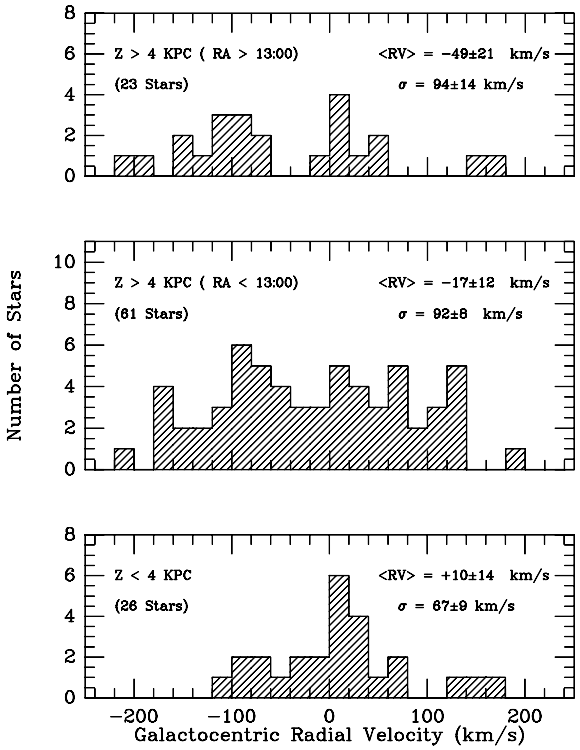

Figure 3. The distributions of galactocentric RV as a function of Z distance above the galactic plane, and at different RA.

method can be used with confidence. Consequently, only Π_{HBP} is used in this paper.

2.3 Radial velocities

The RV for our halo stars were either obtained from spectra obtained at the 4-m Ritchey-Chretien (Kitt Peak National Observatory) and the 3.5-m LRS (TNG) spectrographs or from the literature. A more detailed discussion that includes the sources of these velocities and the individual galactocentric velocities will be given in Kinman et al. (in preparation). The heliocentric RV (with errors) of the program stars are listed in Tables 1 and 2. We have no RV for seven of the RRL stars; these all have $Z > 9$ kpc.

In this analysis, we determine galactocentric radial velocities (RV_{gal}) by assuming a solar motion of $(U, V, W)_{\odot} = (10.0, 5.25, 7.17)$ km s^{-1} with respect to the LSR (Dehnen & Binney 1998) and an LSR velocity of 220 km s^{-1}. The mean galactocentric RV and their corrected dispersions[4] are given in Table 3; their distributions are shown in Fig. 3. We divide our sample of stars into those that lie below and above $Z = 4$ kpc; the group with $Z < 4$ kpc does have a smaller dispersion, but the difference is only significant at the 95 per cent level. There are eight stars in the $Z < 4$ kpc sample that have a $\langle RV_{gal} \rangle$ of $+14.8$ km s^{-1} and a dispersion of only 4.2 km s^{-1}; a W test (Shapiro & Wilk 1965) of the whole $Z < 4$ kpc sample, however, shows no departure from a Gaussian distribution. The dispersions found for the sample with $Z > 4$ kpc are in general agreement with those found for halo stars by Clewley et al. (2004), i.e. 108 ± 10 km s^{-1} at distances 11–52 kpc from the Sun, and by Sirko et al. (2004a) i.e. 99.4 ± 4.3 km s^{-1} for their stars out to 30 kpc. They are, however, smaller than the dispersion of 120 km s^{-1} (out to 30 kpc) found by Battaglia et al. (2005).

The velocity distribution should be Gaussian with a zero mean velocity (Harding et al. 2001) but our $Z > 4$ kpc sample has a mean galactocentric RV of -26.1 ± 10.7 km s^{-1} and an excess of large negative velocities. This excess is most pronounced for the 23 stars whose RA $> 13^{h}$ and whose mean galactocentric RV is -49 ± 21 km s^{-1}. Individually, the two samples with right ascension (RA) greater and less than $13^{h}00^{m}$ show no significant departure from a Gaussian distribution on a W test (Shapiro & Wilk 1965).

2.4 Proper motions and their errors

The proper motions are derived from the plate material used for the construction of the GSC-II catalogue (Lasker et al. 1995; McLean et al. 2000). We used multi-epoch positions that were derived from digitized Schmidt plates from the POSS-I, Quick-V and POSS-II surveys (see Tables 4 and 5). These cover a time baseline of about 40 yr and should allow us to get a precision of a few mas per year.

Table 4. Field centres of the POSS-I and Quick-V Schmidt plates ($6\overset{\circ}{.}4 \times 6\overset{\circ}{.}4$) used in the proper motion determinations.

Field	RA (○)	Dec. (○)	Epoch POSS-I O[a]	Epoch POSS-I E[b]	Epoch Quick-V[c]
266	183.82	35.19	1956.350	1956.349	1983.133
267	190.76	35.20	1950.365	1950.364	1983.133
268	197.69	35.22	1950.367	1950.368	1983.133
320	183.83	29.19	1955.293	1955.293	1983.293
321	190.28	29.20	1950.275	1950.275	1983.293
322	196.73	29.22	1955.288	1955.287	1982.386
323	203.18	29.25	1950.428	1950.425	1982.387

[a]Photographic O band (103aO unfiltered).
[b]Photographic E band (103aE+red Plexiglass 2444).
[c]Photographic V_{12} band (IIaD + Wratten 12).

Table 5. Field centres of the POSS-II Schmidt plates ($6\overset{\circ}{.}4 \times 6\overset{\circ}{.}4$) that were used for the second epoch positions in the proper motion determinations.

Field	RA (○)	Dec. (○)	Epoch POSS-II J[a]	Epoch POSS-II F[b]	Epoch POSS-II N[c]
379	180.64	34.72	1996.216	1989.042	1998.373
380	186.62	34.72	1991.184	1991.184	1995.381
381	192.60	34.73	1990.211	1990.211	1995.384
382	198.58	34.74	1988.279	1989.026	1990.343
441	184.63	29.72	1993.285	1993.217	1996.312
442	190.36	29.73	1990.225	1990.225	1990.080
443	196.10	29.73	1995.233	1995.233	1993.288
444	201.83	29.74	1995.307	1995.307	1998.376

[a]Photographic B_J band (IIIaJ+GG385).
[b]Photographic R_F band (IIIaF+RG610).
[c]Photographic I_N band (IV-N +RG9).

[4] The method of correction is given in Section 3.1.

Table 6. Comparison of our proper motions (O) with those from the *Hipparcos* (H) and Tycho (T) proper motions as given in the NOMAD catalogue Zacharias et al. (2004).

ID (1)	μ_α (2)	μ_δ (3)	Source (4)	μ_α (5)	μ_δ (6)	Source (7)	$\Delta\,\mu_\alpha$ (8)	$\Delta\,\mu_\delta$ (9)
AF-113	-25.9 ± 1.9	-35.8 ± 1.7	O	-26.3 ± 0.9	-33.8 ± 0.8	T	$+0.4 \pm 2.1$	-2.0 ± 1.9
SA57-007	-13.9 ± 1.6	-28.5 ± 2.2	O	-13.1 ± 0.8	-24.1 ± 1.1	T	-0.8 ± 1.8	-4.4 ± 2.5
AF-848	-09.8 ± 3.0	-18.0 ± 2.8	O	-11.8 ± 0.7	-20.5 ± 0.9	T	$+2.0 \pm 3.1$	$+2.5 \pm 2.9$
AF-914	-36.2 ± 3.4	-15.0 ± 3.4	O	-30.5 ± 0.7	-13.1 ± 0.7	T	-5.7 ± 3.5	-1.9 ± 3.5
S-Com	-19.6 ± 4.4	-18.4 ± 3.9	O	-16.4 ± 3.4	-16.5 ± 2.2	H	-3.2 ± 5.6	-1.9 ± 4.5
U-Com	-49.7 ± 2.7	-16.4 ± 2.1	O	-44.4 ± 3.6	-13.8 ± 2.0	H	-5.3 ± 4.5	-2.6 ± 2.9

We used the procedure described by Spagna et al. (1996) to get the *relative* proper motions. These were then transformed to the *absolute* reference frame by forcing the extended extragalactic sources in the field to have no tangential motion. The expected zero point accuracy is $\leqslant 1$ mas yr^{-1}. The proper motions and their individual errors for our program objects are listed in Tables 1 and 2; their formal rms errors are $\leqslant 3$ mas yr^{-1}. Although these proper motions derived from the GSC-II are among the most accurate that are available for the large-field surveys, since an error of 3 mas yr^{-1} corresponds to 14.2 km s^{-1} at 1 kpc, the errors in the computed space motions of halo stars from their proper motions alone will be comparable with the space motions themselves at a distance of $\sim$10 kpc.

Proper motions for six of our brightest program stars are also given in the *Hipparcos* and Tycho catalogues (available in the NOMAD catalogue; Zacharias et al. 2004). These proper motions are compared in Table 6 where it is seen that the differences are largely within the expected errors. These bright stars have large images on our survey plates and probably have the poorest proper motions in our survey. Consequently, this comparison will give limited information on the systematic errors that may be present in our whole survey. It is therefore crucial to have another independent estimate of the size of the proper motion errors. We therefore selected some 74 QSO brighter than 18th magnitude that were listed in our fields by Hewitt & Burbidge (1993) and Véron-Cetty & Véron (2001) and 62 type-C (compact) objects from the Kiso Schmidt Survey for UV-excess galaxies (Takase & Miyauchi-Isobe 1993). These compact UV-excess galaxies have sufficiently 'stellar' images for them to be suitable for use as positional standards. As we noted previously (Kinman et al. 2003), some of these QSO showed surprisingly large proper motions ($\geqslant$10 mas yr^{-1}) and spectra (kindly taken by Arjun Dey and Buell Jannuzi with the Kitt Peak 4.0-m telescope) showed that five of them were stars. We therefore rejected 15 of these objects whose proper motions (in either coordinate) were more than 10 mas yr^{-1}. Table 7 gives the mean proper motion in each field for the remaining 121 objects. The fields are defined by the ID number of the POSS-II and -I plates and some fields are labelled with an 'a' or 'b' in order to identify partially overlapping POSS plates. Objects that fall on overlapping fields have multiple measures; these have been considered as separate measures. The unweighted mean of these 122 independent measures is given as 'All' in Table 7 and is zero within its errors. The rms uncertainty of this result is $\sim$0.3 mas yr^{-1} in each coordinate. Some 86 per cent of the QSO and compact galaxies and 81 per cent of the program stars are in the five fields 381a-267, 382-268, 441-320, 442-321 and 443-322. The unweighted means of the proper motions for these five fields are also zero within their errors. While we cannot be certain that there are not larger systematic errors in individual fields, the available data indicate that the rms systematic error in the proper motion is $\sim$0.3 mas yr^{-1} in each coordinate for the data as a whole.

Table 7. Proper motion systematic errors from QSO and Galaxies. The field identification in Column 1 shows the ID numbers of the POSS-II and -I plates. Column 4 lists the number of QSO+Galaxies (Q+G) measures, and Column 5 lists the number of BHB+RRL stars present in the corresponding fields.

Field	$\mu_\alpha \pm$ err (mas yr^{-1})	$\mu_\delta \pm$ err (mas yr^{-1})	No of Q+G	No of stars
379-266	$\cdots$	$\cdots$	$\cdots$	8
380a-267	$-3.0 \pm \cdots$	$-2.0 \pm \cdots$	1	5
380b-266	$-2.0 \pm \cdots$	$+4.0 \pm \cdots$	1	4
381a-267	-1.68 ± 0.73	-0.81 ± 1.35	9	11
381b-268	$+0.27 \pm 1.36$	-0.29 ± 1.15	7	1
382-268	-0.37 ± 0.87	$+0.49 \pm 0.73$	23	9
441-320	-0.24 ± 0.70	$+0.84 \pm 0.95$	14	28
442-321	$+0.27 \pm 0.50$	-0.66 ± 0.59	30	26
443-322	$+0.16 \pm 0.62$	-0.37 ± 0.69	29	21
444a-322	$\cdots$	$\cdots$	$\cdots$	1
444b-323	-1.56 ± 0.74	$+0.78 \pm 1.26$	8	3
All	-0.25 ± 0.28	-0.07 ± 0.31	122	117
Five fields	-0.14 ± 0.31	-0.14 ± 0.34	105	95

The extragalactic standards are somewhat fainter on average than the program stars so that we must also be aware that magnitude-dependent errors may also be present.

3 ANALYSIS AND RESULTS

3.1 The space velocities *U*, *V* and *W*

The heliocentric space velocity components ***U, V*** and ***W*** were derived from the data listed in Tables 1 and 2. We used the program by Johnson & Soderblom (1987) (updated for the J2000 reference frame and further updated with the transformation matrix derived from vol. 1 of the *Hipparcos* data catalogue). This program gives a right-handed system for ***U***, ***V*** and ***W*** in which these vectors are positive towards the directions of the Galactic centre, Galactic rotation and the NGP, respectively.[5] As noted in Sections 2.2.2 and 2.2.3, $\Pi_{\rm HBP}$ and Π_V were adopted for the parallaxes of the BHB and RRL stars, respectively. No RV are yet available for seven of the RRL stars. We therefore assumed, when calculating their ***U***, ***V*** and ***W*** velocities, that their RV is zero with an error of 150 km s^{-1}. This should give acceptable ***U*** and ***V*** velocities since these depend almost entirely on the proper motions; their ***W*** velocities must, of course, be discarded. These values of ***U***, ***V*** and ***W*** together with the

[5] Other authors (e.g. Majewski 1992) use a left-handed system in which ***U*** is positive towards the Galactic anticentre.

height (Z) of the star above the Galactic plane and the galactocentric distance ($R_{\rm gal}$) are given in Tables 8 and 9 for the BHB and RRL stars, respectively. We assume a solar galactocentric distance of 8.0 kpc.

Table 10 gives the mean values $\langle U\rangle$, $\langle V\rangle$ and $\langle W\rangle$ of these space velocities for various ranges of Z. The mean values and dispersion given in parentheses were obtained by trimming the 10 per cent of the sample that have the most extreme values. This has little effect on the mean values and will not be discussed further. The rms dispersions in these quantities must be corrected for the errors in the individual $\boldsymbol{U}$, $\boldsymbol{V}$ and $\boldsymbol{W}$ space velocities (given in Tables 8 and 9). Following Jones & Walker (1988), if the observed dispersion in

Table 8. The BHB stars of our sample. The $\boldsymbol{U}$, $\boldsymbol{V}$ and $\boldsymbol{W}$ velocities (in km s^{-1}) are heliocentric. The velocities $\boldsymbol{V}_r$, $\boldsymbol{V}_\phi$ and $\boldsymbol{V}_z$ (in km s^{-1}) are in galactocentric cylindrical coordinates. For further details see text.

ID (1)	Z (kpc) (2)	$R_{\rm gal}$ (kpc) (3)	$\boldsymbol{U}$ (4)	$\boldsymbol{V}$ (5)	$\boldsymbol{W}$ (6)	$\boldsymbol{V}_R$ (7)	$\boldsymbol{V}_\phi$ (8)	$\boldsymbol{V}_z$ (9)
16549-51	3.6	9.5	−192 ± 033	−246 ± 026	+007 ± 049	−183 ± 033	−013 ± 026	−014 ± 049
AF-003	14.8	18.5	+199 ± 296	−209 ± 323	−039 ± 071	+207 ± 296	+028 ± 323	+032 ± 071
AF-006	3.2	9.1	+011 ± 048	−338 ± 042	+013 ± 013	+022 ± 048	−106 ± 042	−020 ± 013
AF-011	10.0	14.1	+418 ± 198	−534 ± 277	−021 ± 037	+432 ± 198	−295 ± 277	+014 ± 037
AF-013	15.6	18.9	−130 ± 153	−405 ± 127	+084 ± 048	−106 ± 153	−183 ± 127	−091 ± 048
AF-727	4.3	9.9	+048 ± 033	−024 ± 036	−012 ± 012	+062 ± 033	+206 ± 036	+005 ± 012
AF-022	12.6	16.2	+072 ± 114	−370 ± 082	−037 ± 022	+085 ± 114	−136 ± 082	+030 ± 022
AF-729	8.0	12.5	+021 ± 072	−331 ± 074	−016 ± 041	+027 ± 072	−100 ± 074	+009 ± 041
AF-029	6.6	11.4	+079 ± 081	−105 ± 064	−045 ± 017	+090 ± 081	+125 ± 064	+038 ± 017
AF-030	5.8	10.6	−077 ± 063	−324 ± 059	+016 ± 014	−065 ± 063	−094 ± 059	−023 ± 014
16022-26	5.8	10.5	+013 ± 050	−288 ± 065	−047 ± 049	+025 ± 050	−055 ± 065	+040 ± 049
AF-038	8.7	12.8	−078 ± 089	−423 ± 127	−090 ± 017	−070 ± 089	−191 ± 127	+083 ± 017
AF-039	12.2	15.7	−280 ± 091	−217 ± 094	+011 ± 041	−271 ± 091	+006 ± 094	−018 ± 041
AF-041	7.4	11.8	−148 ± 058	−433 ± 066	+077 ± 013	−141 ± 058	−200 ± 066	−084 ± 013
AF-045	3.4	9.1	−055 ± 019	−067 ± 020	+007 ± 010	−049 ± 019	+164 ± 020	−014 ± 010
AF-046	11.0	14.6	−136 ± 112	−192 ± 162	+040 ± 017	−128 ± 112	+036 ± 162	−047 ± 017
AF-048	3.6	9.3	−038 ± 034	−211 ± 037	+018 ± 011	−029 ± 034	+021 ± 037	−025 ± 011
AF-050	15.2	18.3	+042 ± 216	−384 ± 180	+019 ± 050	+059 ± 216	−149 ± 180	−026 ± 050
AF-052	6.0	10.7	−116 ± 110	−293 ± 090	−088 ± 018	−106 ± 110	−062 ± 090	+081 ± 018
AF-053	6.8	11.4	+148 ± 059	−402 ± 091	+047 ± 015	+153 ± 059	−173 ± 091	−054 ± 015
AF-063	12.4	15.6	−079 ± 096	−316 ± 075	−117 ± 015	−069 ± 096	−085 ± 075	+110 ± 015
16026-28	3.2	8.9	+033 ± 024	−055 ± 022	−085 ± 010	+038 ± 024	+178 ± 022	+078 ± 010
AF-754	7.8	12.2	+012 ± 077	−252 ± 120	+008 ± 045	+019 ± 077	−021 ± 120	−015 ± 045
AF-755	7.8	12.2	−031 ± 098	−296 ± 113	−101 ± 044	−027 ± 098	−062 ± 113	+094 ± 044
AF-068	5.8	10.4	−001 ± 065	−195 ± 052	−136 ± 012	+008 ± 065	+037 ± 052	+129 ± 012
AF-070	6.9	11.1	−094 ± 052	−231 ± 066	+166 ± 011	−085 ± 052	−001 ± 066	−173 ± 011
AF-073	16.8	19.6	+233 ± 125	−238 ± 122	−001 ± 042	+241 ± 125	−023 ± 122	−006 ± 042
AF-075	8.3	12.1	+231 ± 103	−365 ± 089	−020 ± 014	+238 ± 103	−137 ± 089	+013 ± 014
AF-076	9.9	13.3	+065 ± 102	−285 ± 066	+046 ± 013	+074 ± 102	−054 ± 066	−053 ± 013
AF-077	9.2	12.9	+175 ± 146	−329 ± 166	−126 ± 022	+180 ± 146	−104 ± 166	+119 ± 022
AF-078	4.4	9.5	+118 ± 027	−087 ± 037	−165 ± 010	+128 ± 027	+144 ± 037	+158 ± 010
AF-769	3.5	9.1	−116 ± 036	−393 ± 046	+021 ± 011	−112 ± 036	−158 ± 046	−028 ± 011
16026-67	2.9	8.6	−041 ± 037	−338 ± 055	−040 ± 010	−031 ± 037	−106 ± 055	+033 ± 010
AF-100	3.9	9.1	−181 ± 032	−305 ± 040	+049 ± 010	−172 ± 032	−072 ± 040	−056 ± 010
16466-08	6.3	10.7	−123 ± 076	−257 ± 062	+025 ± 040	−115 ± 076	−018 ± 062	−032 ± 040
AF-108	3.8	9.0	−072 ± 032	−492 ± 046	−069 ± 010	−064 ± 032	−260 ± 046	+062 ± 010
AF-111	5.0	9.8	−282 ± 047	−087 ± 045	−037 ± 011	−266 ± 047	+157 ± 045	+030 ± 011
AF-112	2.6	8.6	+069 ± 023	−089 ± 022	+009 ± 010	+080 ± 023	+142 ± 022	−016 ± 010
AF-113	1.6	8.3	−025 ± 014	−341 ± 019	+020 ± 010	−017 ± 014	−109 ± 019	−027 ± 010
AF-115	8.1	11.9	−017 ± 060	−397 ± 056	+041 ± 011	−020 ± 060	−164 ± 056	−048 ± 011
16466-15	2.9	8.7	−052 ± 042	−079 ± 052	+146 ± 011	−040 ± 042	+154 ± 052	−153 ± 011
AF-130	11.4	14.2	+063 ± 090	−209 ± 068	+113 ± 010	+073 ± 090	+021 ± 068	−120 ± 010
AF-131	9.2	12.6	−012 ± 080	−314 ± 078	+059 ± 011	−007 ± 080	−082 ± 078	−066 ± 011
AF-134	2.6	8.6	+220 ± 023	−204 ± 019	+002 ± 109	+230 ± 023	+023 ± 019	−009 ± 010
16031-44	4.2	9.1	+161 ± 040	−203 ± 056	+011 ± 010	+170 ± 040	+030 ± 056	−018 ± 010
15622-48	5.7	9.9	+078 ± 049	−279 ± 064	−069 ± 010	+087 ± 049	−047 ± 064	+062 ± 010
15622-07	2.7	8.5	+033 ± 033	−172 ± 039	−037 ± 010	+042 ± 033	+060 ± 039	+030 ± 010
AF-138	5.2	9.8	−053 ± 065	−325 ± 059	+124 ± 011	−049 ± 065	−091 ± 059	−131 ± 011
15622-09	3.0	8.5	+086 ± 025	−178 ± 032	−122 ± 010	+095 ± 025	+054 ± 032	+115 ± 010
AF-797	8.1	12.0	−144 ± 072	−350 ± 050	+119 ± 039	−149 ± 072	−100 ± 050	−126 ± 039
AF-804	4.5	9.5	−174 ± 043	−243 ± 034	+114 ± 010	−165 ± 043	+002 ± 034	−121 ± 010
SA57-001	5.7	9.9	+228 ± 069	−445 ± 060	−113 ± 010	+234 ± 069	−216 ± 060	+106 ± 010
SA57-006	4.4	9.2	−191 ± 053	−257 ± 050	+119 ± 010	−183 ± 053	−021 ± 050	−126 ± 010
SA57-007	1.6	8.2	+030 ± 013	−240 ± 026	−084 ± 049	+039 ± 013	−008 ± 026	+077 ± 049

Table 8 – *continued*

ID (1)	Z (kpc) (2)	$R_{\rm gal}$ (kpc) (3)	$\boldsymbol{U}$ (4)	$\boldsymbol{V}$ (5)	$\boldsymbol{W}$ (6)	$\boldsymbol{V}_R$ (7)	$\boldsymbol{V}_\phi$ (8)	$\boldsymbol{V}_z$ (9)
SA57-009	11.8	14.3	-169 ± 136	-716 ± 117	$+067 \pm 010$	-181 ± 136	-477 ± 117	-074 ± 010
SA57-017	3.3	8.6	-239 ± 069	-356 ± 063	$+004 \pm 010$	-231 ± 069	-122 ± 063	-011 ± 010
SA57-021	10.3	13.2	-399 ± 134	$+066 \pm 146$	-085 ± 042	-358 ± 134	$+336 \pm 146$	$+078 \pm 042$
SA57-029	12.6	15.0	-009 ± 099	-307 ± 105	-161 ± 040	-008 ± 099	-075 ± 105	$+154 \pm 040$
SA57-032	7.8	11.3	-074 ± 069	-406 ± 084	$+017 \pm 012$	-078 ± 069	-169 ± 084	-024 ± 012
SA57-036	11.9	14.3	$+003 \pm 123$	-398 ± 141	$+012 \pm 011$	$+001 \pm 123$	-166 ± 141	-019 ± 011
SA57-040	7.4	10.8	-033 ± 049	-128 ± 046	$+036 \pm 010$	-019 ± 049	$+105 \pm 046$	-043 ± 010
SA57-041	13.0	15.1	-124 ± 115	-341 ± 114	$+146 \pm 011$	-124 ± 115	-099 ± 114	-153 ± 011
SA57-045	8.2	11.5	$+206 \pm 050$	-242 ± 045	-113 ± 010	$+213 \pm 050$	-030 ± 045	$+106 \pm 010$
AF-825	4.8	9.5	-040 ± 023	-191 ± 030	-114 ± 049	-027 ± 023	$+043 \pm 030$	$+107 \pm 049$
SA57-046	16.1	17.7	-111 ± 143	-483 ± 157	$+174 \pm 040$	-123 ± 143	-241 ± 157	-181 ± 040
SA57-055	11.6	14.0	$+136 \pm 141$	-315 ± 102	-201 ± 014	$+134 \pm 141$	-100 ± 103	$+194 \pm 014$
AF-841	4.5	9.2	-012 ± 029	-273 ± 035	$+006 \pm 010$	-006 ± 029	-041 ± 035	-013 ± 010
AF-848	1.4	8.1	$+014 \pm 019$	-144 ± 021	-099 ± 010	$+025 \pm 019$	$+088 \pm 021$	$+092 \pm 010$
SA57-066	6.1	10.0	-009 ± 087	-168 ± 075	-225 ± 013	$+005 \pm 087$	$+064 \pm 075$	$+218 \pm 013$
AF-854	6.9	10.9	-295 ± 058	-211 ± 052	$+019 \pm 049$	-279 ± 058	$+067 \pm 052$	-026 ± 049
SA57-080	4.6	9.1	-083 ± 038	-192 ± 048	-024 ± 010	-072 ± 038	$+044 \pm 048$	$+017 \pm 010$
AF-866	4.1	9.0	$+030 \pm 042$	-245 ± 050	-003 ± 050	$+038 \pm 042$	-016 ± 050	-004 ± 050
SA57-087	10.9	13.4	-077 ± 135	-308 ± 135	-074 ± 018	-079 ± 135	-064 ± 135	$+067 \pm 018$
AF-900	3.4	8.6	-018 ± 020	-215 ± 025	$+128 \pm 049$	-008 ± 020	$+018 \pm 025$	-135 ± 049
SA57-111	13.6	15.4	-160 ± 089	-448 ± 094	-080 ± 014	-191 ± 089	-181 ± 094	$+073 \pm 014$
AF-909	7.0	10.4	$+060 \pm 042$	-214 ± 043	-121 ± 011	$+071 \pm 042$	$+010 \pm 043$	$+114 \pm 011$
AF-914	1.7	8.2	-162 ± 031	-249 ± 037	$+151 \pm 049$	-154 ± 031	-010 ± 037	-158 ± 049
AF-916	4.7	9.2	$+073 \pm 033$	-130 ± 036	-115 ± 049	$+091 \pm 033$	$+094 \pm 036$	$+108 \pm 049$
AF-918	4.1	8.7	-055 ± 041	-188 ± 039	$+001 \pm 049$	-043 ± 041	$+047 \pm 039$	-008 ± 049

U is Disp (U), and ξ_i is the error in U of star i, then the corrected dispersion σ_u is given by

$$\sigma_u^2 = (\mathrm{Disp}(U))^2 - \frac{1}{n}\sum_{i=1}^{n}\xi_i^2 \qquad (7)$$

and similarly for the space velocities $\boldsymbol{V}$ and $\boldsymbol{W}$. These corrected dispersions are given in Columns 5, 7 and 10 of Table 10. For a given proper motion error, the space velocity error ξ_i increases with distance; when it becomes comparable with the intrinsic velocity dispersion (at $Z \sim 10$ kpc), the correction becomes unreliable. Table 10 also gives $\langle U\rangle$, $\langle V\rangle$ and $\langle W\rangle$ and their dispersions for three halo samples from the solar neighbourhood. Local A is a sample of stars that were confirmed as BHB stars by high-resolution spectroscopy (Kinman et al. 2000); these stars have *Hipparcos* proper motions and RV with errors of a few km s^{-1}; their parallaxes and space velocities were determined in exactly the same way as for our program BHB stars. Local B is the HALO1 sample of local RRL stars (with [Fe/H] < -1.3) from Martin & Morrison (1998). Local C is their HALO2 sample in which the total space velocity (which is defined by equation 8 in Section 3.4) was used to exclude thick disc stars (as shown in our Fig. 6). Martin & Morrison used $M_V = +0.73$ (at [Fe/H] $= -1.9$) to determine the distances of their RRL stars; they plot the *U, V* and *W* and their dispersions for their HALO2 sample as a function of M_V in figs 6 and 7, respectively, of *their paper*. We used these plots to derive the space motions of their HALO2 sample for our assumed M_V of $+0.54$ at [Fe/H] $= -1.5$; these are given as Local D. Changes in M_V have the greatest effect on the $\boldsymbol{V}$ space velocity and the $\boldsymbol{U}$ velocity dispersion in these *local* halo samples.

If we assume that $\langle V_{\rm LSR}\rangle = -220$ km s^{-1} for zero halo rotation, the corresponding $\langle V_{\rm hel}\rangle$ will be ~ -225 km s^{-1} (see Section 2.3). Older *local* halo samples (see table 5 of Martin & Morrison) show slightly prograde $\langle V\rangle$. It is not clear how much these prograde $\langle V\rangle$ are a result of the adopted distance scales and/or the presence of disc stars in these halo samples. Most *local* samples have the problem that either (i) they may contain some thick-disc stars (as in the case of the HALO1) or (ii) they may have some kinematic bias which is introduced in the attempt to remove the disc component (e.g. HALO2) or which is present in their original selection (e.g. Local A). The differences between the space motions of the different local samples suggest that these putative systematic sampling errors are comparable in size to their statistical errors.

3.2 The halo rotation $\langle V\rangle$

We see in Table 10 that the mean value $\langle V\rangle$ of our halo sample becomes increasingly *negative* (corresponding to more retrograde orbits) with increasing height Z above the galactic plane. This change in $\langle V\rangle$ is several times its calculated error and so is formally significant. The V of the individual stars are shown as a function of Z in Fig. 4(c); a line connects the $\langle V\rangle$ in this plot. The halo stars with $0 < Z < 4$ kpc ($\langle Z\rangle = 2.8$ kpc) have $\langle V\rangle = -242 \pm 22$ km s^{-1}. This is compatible with them having (on average) zero rotation; it is those with $4 < Z < 8$ kpc that have an excess of retrograde orbits. Figs 4(a) and (b) include only stars with $Z < 8$ kpc and are to be compared with stars in the same Z-range shown in figs 1(c) and (b), respectively, in MMH which are in the SA57 at the NGP. The vertical dotted line in Fig. 4(a) and MMH (fig. 1c) is the demarcation between prograde and retrograde orbits. Both plots show a number of very retrograde orbits with negative $\boldsymbol{W}$ velocities. The pronounced correlation between U and W in MMH (fig. 1b) is present to a lesser extent in Fig. 4(b).[6] There is therefore qualitative agreement with MMH that there is

[6] The different sign convention for $\boldsymbol{U}$ used by MMH causes negative $\boldsymbol{U}$ to correlate with negative $\boldsymbol{W}$ in their case and positive $\boldsymbol{W}$ in our case.

Table 9. The RRL stars of our sample. The $\boldsymbol{U}$, $\boldsymbol{V}$ and $\boldsymbol{W}$ velocities (in km s^{-1}) are heliocentric. The velocities $\boldsymbol{V}_R$, $\boldsymbol{V}_\phi$ and $\boldsymbol{V}_z$ (in km s^{-1}) are in galactocentric cylindrical coordinates. For further details see text.

ID (1)	Z (kpc) (2)	$R_{\rm gal}$ (kpc) (3)	$\boldsymbol{U}$ (4)	$\boldsymbol{V}$ (5)	$\boldsymbol{W}$ (6)	$\boldsymbol{V}_R$ (7)	$\boldsymbol{V}_\phi$ (8)	$\boldsymbol{V}_z$ (9)
GR-Com	13.9	17.3	−035 ± 095	−470 ± 111	···	−001 ± 095	−239 ± 111	···
GH-Com	8.9	13.0	+113 ± 076	−373 ± 096	···	+133 ± 076	−131 ± 096	···
IQ-Com	10.4	14.2	−144 ± 086	−137 ± 065	···	−142 ± 086	+084 ± 065	···
NSV5476	7.4	12.0	+011 ± 062	−332 ± 051	−019 ± 050	+019 ± 062	−100 ± 051	+012 ± 050
V-Com	3.4	9.2	−221 ± 086	−133 ± 153	−018 ± 028	−215 ± 086	+092 ± 153	+011 ± 028
CD-Com	9.4	13.4	−233 ± 068	−703 ± 085	−257 ± 014	−214 ± 068	−475 ± 085	+250 ± 014
AF-031	9.5	13.4	−133 ± 072	−444 ± 124	−202 ± 050	−118 ± 072	−215 ± 124	+195 ± 050
TU-Com	4.4	9.7	+194 ± 095	−368 ± 168	−074 ± 016	+204 ± 095	−134 ± 168	+067 ± 016
CK-Com	6.6	11.3	+047 ± 042	−557 ± 049	−070 ± 012	+051 ± 042	−326 ± 049	+063 ± 012
AF-042	14.1	17.3	−099 ± 151	−363 ± 141	···	−083 ± 151	−135 ± 141	···
CL-Com	7.7	11.9	+076 ± 083	−207 ± 050	−025 ± 016	+085 ± 083	+026 ± 050	+018 ± 016
AT-CVn	6.8	11.4	−089 ± 086	−266 ± 121	+089 ± 052	−081 ± 086	−032 ± 121	−096 ± 052
GY-Com	11.4	14.8	+293 ± 089	−204 ± 095	···	+300 ± 089	+044 ± 095	···
GS-Com	14.8	17.6	+111 ± 186	−335 ± 293	···	+126 ± 187	−095 ± 293	···
RR-CVn	2.6	8.8	−053 ± 031	−390 ± 040	+014 ± 011	−047 ± 031	−157 ± 040	−021 ± 011
S-Com	1.7	8.3	−055 ± 034	−205 ± 033	−066 ± 004	−046 ± 034	+027 ± 033	+059 ± 004
SV-CVn	2.7	8.8	+090 ± 018	−326 ± 028	+081 ± 028	+095 ± 018	−098 ± 028	−088 ± 028
FV-Com	6.5	10.7	+180 ± 060	−154 ± 061	−171 ± 050	+190 ± 060	+076 ± 061	+164 ± 050
U-Com	1.7	8.2	−264 ± 020	−314 ± 019	−038 ± 003	−255 ± 020	−083 ± 019	+031 ± 003
SW-CVn	2.8	8.8	−157 ± 036	−200 ± 036	−012 ± 021	−146 ± 036	+038 ± 036	+005 ± 021
DV-Com	7.3	11.0	+280 ± 066	−316 ± 086	−127 ± 010	+289 ± 066	−083 ± 086	+120 ± 010
AF-791	6.9	11.0	−362 ± 061	−036 ± 054	−230 ± 012	−334 ± 061	+226 ± 054	+223 ± 012
AW-Com	10.5	13.4	+235 ± 072	−145 ± 092	···	+246 ± 072	+080 ± 092	···
TX-Com	5.6	10.0	+236 ± 052	−357 ± 048	−088 ± 049	+240 ± 052	−134 ± 048	+081 ± 049
AP-CVn	4.6	9.5	−181 ± 038	−247 ± 044	−009 ± 049	−173 ± 038	−007 ± 044	+002 ± 049
EM-Com	9.5	12.6	+152 ± 102	−334 ± 087	−105 ± 010	+155 ± 102	−111 ± 087	+098 ± 010
AF-155	7.8	11.5	+018 ± 083	−262 ± 090	−098 ± 032	+025 ± 083	−032 ± 090	+091 ± 032
TY-CVn	4.0	9.1	−359 ± 048	−303 ± 058	+084 ± 016	−353 ± 048	−057 ± 058	−091 ± 016
IP-Com	7.2	10.8	+157 ± 087	−471 ± 100	−111 ± 030	+155 ± 087	−246 ± 100	+104 ± 030
SA57-19	6.4	10.2	−110 ± 049	−364 ± 052	+059 ± 050	−104 ± 049	−130 ± 052	−066 ± 050
EO-Com	6.9	10.6	−154 ± 078	−459 ± 064	+089 ± 010	−153 ± 078	−222 ± 064	−096 ± 010
UV-Com	10.1	12.9	−293 ± 067	−314 ± 084	+076 ± 011	−290 ± 067	−059 ± 084	−083 ± 011
TZ-CVn	5.3	9.7	+165 ± 075	−361 ± 074	−131 ± 050	+166 ± 075	−139 ± 074	+124 ± 050
SA57-47	5.9	9.8	+137 ± 054	−701 ± 067	−134 ± 037	+128 ± 054	−474 ± 067	+127 ± 037
SA57-60	5.4	9.4	−020 ± 058	−473 ± 068	−090 ± 050	−017 ± 058	−241 ± 068	+083 ± 050
EW-Com	8.0	11.2	−220 ± 063	−239 ± 074	+050 ± 012	−211 ± 063	+015 ± 074	−057 ± 012
IS-Com	4.4	8.9	−047 ± 032	−440 ± 044	−132 ± 010	−045 ± 032	−207 ± 044	+125 ± 010
AF-882	6.3	10.3	+043 ± 047	−286 ± 050	−071 ± 050	+044 ± 047	−061 ± 050	+064 ± 050

structure in the phase space distribution of these NGP stars. We test this quantitatively in the next section.

3.3 Is our NGP halo sample homogeneous?

Table 11 gives $\langle U\rangle$ and $\langle V\rangle$ and their corrected dispersions σ_u and σ_v for our 78 halo stars with $Z < 8$ kpc. Separate solutions are given for the RRL and BHB stars and also for the stars with positive and negative $\boldsymbol{W}$ space velocities. These show the following.

(i) The combined solution for $\langle V\rangle$ for both RRL and BHB stars and all W (-268 ± 14 km s^{-1}) is in good agreement with that found by Majewski (1992) (-275 km s^{-1}). The $\langle V\rangle$ of the BHB stars alone (-239 ± 15 km s^{-1}) is only mildly retrograde and compatible with zero halo rotation. The RRL sample alone, however, is strongly retrograde (-328 ± 28 km s^{-1}). The dispersion σ_v of the 20 RRL stars with negative W (136 ± 21 km s^{-1}) is much greater than that (13 ± 4 km s^{-1}) of the six RRL that have positive W. Despite the rather small numbers, a variance ratio test shows this difference to be significant at better than the 99 per cent level. The distributions of V for the BHB and RRL are shown in Fig. 5. The hatched histograms are for the stars that have negative W velocities. Following Shapiro & Wilk (1965), separate tests of the V-distributions of the BHB and RRL stars with $Z < 8$ kpc show that neither have significant differences from normal distributions.

(ii) There is an asymmetry in the ratio of RRL to BHB stars in the sense that the ratio is larger in the sample that has negative W velocities. This effect is significant at better than the 99 per cent level and suggests that we are not dealing with a homogeneous halo population.

(iii) The $\langle U\rangle$ space velocity is significantly negative (-72 ± 21 km s^{-1}) for both BHB and RRL stars that have positive W velocities. Those with negative W have the expected zero $\langle U\rangle$.

There is therefore strong evidence that the NGP halo stars with $Z < 8$ kpc do not belong to a homogeneous population. It does not seem likely that observational selection in the samples could produce the differences in the kinematic properties between the BHB and RRL stars noted in (ii) above. The RRL stars cover roughly the

Table 10. Mean heliocentric space velocities $\boldsymbol{U}$, $\boldsymbol{V}$ and $\boldsymbol{W}$ (km s^{-1}) for our program BHB and RRL stars as a function of height Z (kpc) above the galactic plane and for local samples of these stars. Local A is a sample of BHB stars (Kinman et al. 2000) and Local B and C are the HALO1 and HALO2 samples of RRL stars (Martin & Morrison 1998). Local D is the HALO2 sample after normalization to our distance scale.

Range in Z	$\langle Z\rangle$	n_{uv}	$\langle U\rangle$	σ_u	$\langle V\rangle$	σ_v	n_w	$\langle W\rangle$	σ_w
(1)	(2)	(3)	(4)	(5)	(6)	(7)	(8)	(9)	(10)
0–4	2.8	26	-52 ± 23 (-55 ± 20)	110 ± 15	-242 ± 22 (-239 ± 20)	103 ± 14	26	0 ± 14 (-1 ± 20)	67 ± 9
4–8	6.0	52	-12 ± 20 (-7 ± 16)	131 ± 13	-282 ± 18 (-278 ± 14)	111 ± 11	52	-37 ± 13 (-37 ± 11)	85 ± 8
8–12	9.8	25	$+1 \pm 41$ $(+7 \pm 36)$	172 ± 24	-328 ± 34 (-328 ± 27)	119 ± 17	21	-32 ± 24 (-28 ± 22)	106 ± 15
$\geqslant$12	14.1	14	-26 ± 40 (-24 ± 36)	...	-349 ± 24 (-350 ± 23)	...	11	0 ± 33 (-2 ± 24)	96 ± 22
Local A	0	27	-1 ± 25	129 ± 18	-210 ± 15	79 ± 11	27	-14 ± 20	101 ± 14
Local B	0	81	-8 ± 20	180 ± 14	-197 ± 12	111 ± 9	81	-8 ± 10	93 ± 7
Local C	0	84	$+1 \pm 21$	193 ± 15	-219 ± 10	91 ± 7	84	-5 ± 10	96 ± 7
Local D	0	84	$+3 \pm 23$	214 ± 17	-240 ± 11	100 ± 8	84	-8 ± 11	108 ± 8

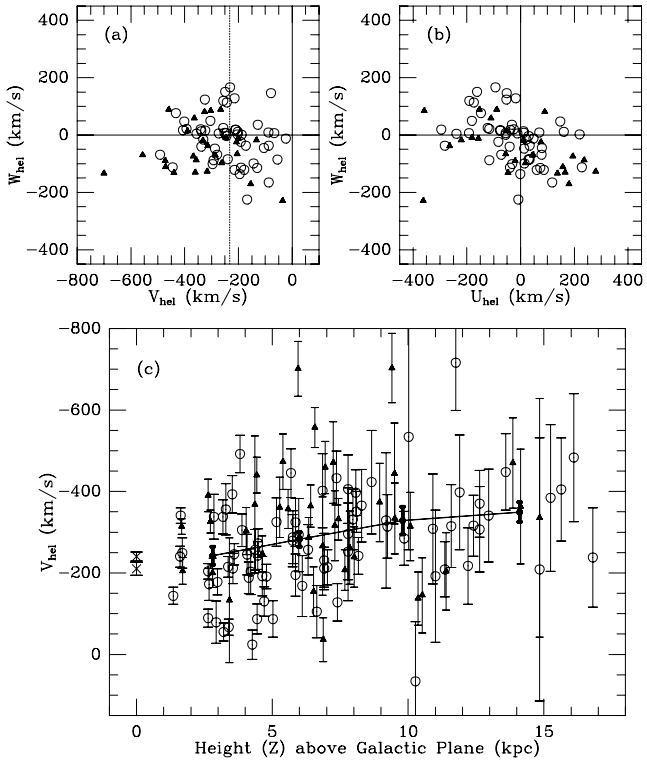

Figure 4. Plots of $V_{\rm hel}$ versus $W_{\rm hel}$ and $U_{\rm hel}$ versus $W_{\rm hel}$ are shown in (a) and (b), respectively, for the stars with $Z < 8$ kpc. The vertical dotted line in (a) divides stars with retrograde orbits (on the left-hand side) from those with prograde orbits. The lower figure (c) plots $V_{\rm hel}$ versus the height (Z) above the galactic plane for the whole sample. The locations of the mean $V_{\rm hel}$ of Local A and D are shown by crosses. Filled triangles and open circles represent the RRL and BHB program stars, respectively; the line connects the values of $\langle V\rangle$ for these stars.

same area of the sky as the BHB stars (Fig. 1) and the six RRL with positive W are distributed widely in both RA and Dec. The lack of homogeneity must therefore be present over much of the survey area. We noted in Section 2.3 that stars with RA $> 13^{\rm h}\,00^{\rm m}$ showed predominantly negative RV. There are six RRL stars with these RA and $Z < 8$ kpc. Their heliocentric space velocities and dispersions are

$$\langle U\rangle = +010 \pm 63 \ \text{km s}^{-1} \quad \sigma_u = 128 \pm 37 \ \text{km s}^{-1}$$
$$\langle V\rangle = -417 \pm 74 \ \text{km s}^{-1} \quad \sigma_v = 152 \pm 44 \ \text{km s}^{-1}$$
$$\langle W\rangle = -085 \pm 32 \ \text{km s}^{-1} \quad \sigma_w = 059 \pm 17 \ \text{km s}^{-1}.$$

This small group thus shows a highly retrograde $\langle V\rangle$ and a negative $\langle W\rangle$, but their corrected velocity dispersions are not unusual.

3.4 The RRL sample

The 26 RRL stars with $Z < 8$ kpc have a mean height above the plane of 5.3 kpc. Our analysis of the QSO proper motions gave a rms systematic error in the proper motions of 0.3 mas yr^{-1} in each coordinate. This corresponds to a $\sim$2 km s^{-1} error in V at a distance of 1 kpc. Consequently for our $Z < 8$ kpc sample, a 2σ systematic error in $\langle V\rangle$ from the proper motions should *on average* produce a $\sim$20 km s^{-1} systematic error in V. It does not seem likely therefore that systematic errors in the proper motions can wholly account for the retrograde motion ($\sim$100 km s^{-1}) of the RRL sample. The retrograde V could also be produced if our RRL distances are 45 per cent too large. This corresponds to a 0.8 mag error in the modulus of these stars. We used the same M_V for the RRL stars as for the reddest BHB stars.[7] It does not seem likely therefore that our M_V can have

[7] The 15 BHB stars that have $Z < 8$ kpc and $(B-V) > 0.10$ have $\langle V\rangle = -227 \pm 35$ and $\sigma_v = 116 \pm 21$ km s^{-1}, so they do not show a retrograde motion.

Table 11. Mean heliocentric space velocities $\langle U\rangle$ and $\langle V\rangle$ and the total space velocity $\langle T\rangle$ (km s^{-1}) for our program BHB and RRL stars for different ranges of the space velocity W.

Star type (1)	Range in W (2)	n_{uv} (3)	$\langle U\rangle$ (4)	σ_u (5)	$\langle V\rangle$ (6)	σ_v (7)	$\langle T\rangle$ (8)	σ_T (9)
RRL	$W<0$	20	$+12\pm41$	166 ± 26	-321 ± 36	136 ± 21	403 ± 29	125 ± 19
BHB	$W<0$	24	$+11\pm20$	78 ± 11	-216 ± 24	85 ± 12	272 ± 22	104 ± 15
All	$W<0$	44	$+12\pm21$	124 ± 13	-264 ± 22	128 ± 14	332 ± 20	131 ± 14
RRL	$W>0$	6	-112 ± 41	135 ± 39	-351 ± 31	13 ± 4	410 ± 31	69 ± 20
BHB	$W>0$	28	-64 ± 20	108 ± 14	-258 ± 19	82 ± 11	309 ± 19	96 ± 13
All	$W>0$	34	-72 ± 21	112 ± 14	-275 ± 17	81 ± 10	327 ± 17	99 ± 12
RRL	All W	26	-17 ± 35	165 ± 23	-328 ± 28	118 ± 16	405 ± 23	113 ± 16
BHB	All W	52	-29 ± 16	102 ± 10	-239 ± 15	93 ± 9	292 ± 14	101 ± 10
All	All W	78	-25 ± 16	125 ± 10	-268 ± 14	109 ± 9	329 ± 13	117 ± 9
RRL($P>0.6$ d)	All W	8	-8 ± 66	163 ± 41	-414 ± 75	189 ± 47	490 ± 50	132 ± 33
RRL($P<0.6$ d)	All W	18	-21 ± 44	171 ± 28	-290 ± 21	33 ± 6	374 ± 20	82 ± 14

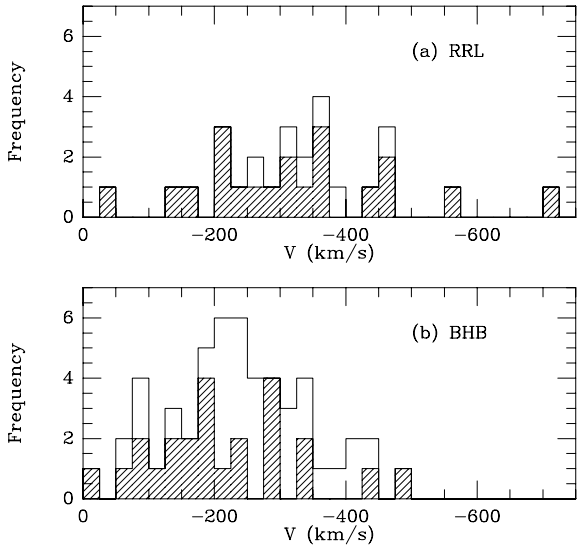

Figure 5. The distributions of V for (a) the RRL stars and (b) the BHB stars in our NGP sample. Stars with hatched histograms are those with negative W velocities.

such a large error. Neither does it seem likely that the mean apparent magnitudes of the RRL stars could have as much systematic error since they are based on multiple photoelectric observations.

The total space velocities (T) of our program stars were calculated from the space velocities $\boldsymbol{U}$, $\boldsymbol{V}$ and $\boldsymbol{W}$ (Tables 8 and 9) by

$$T=\sqrt{\boldsymbol{U}^2+\boldsymbol{V}^2+\boldsymbol{W}^2}. \quad (8)$$

These total space velocities are plotted against the height above the galactic plane (Z) for the BHB stars and RRL stars in Figs 6(a) and (b), respectively. The Local A sample of nearby BHB stars is also plotted as filled squares in Fig. 6(a). The encircled triangles are the RRL stars that have W velocities <-50 km s^{-1}. The line

$$T(\mathrm{km\ s^{-1}})=235-86\times Z \quad (9)$$

shows the boundary that is used by Martin & Morrison to separate their HALO2 from their DISK2 populations; all our program stars belong to their HALO2 population. Most of our stars have values

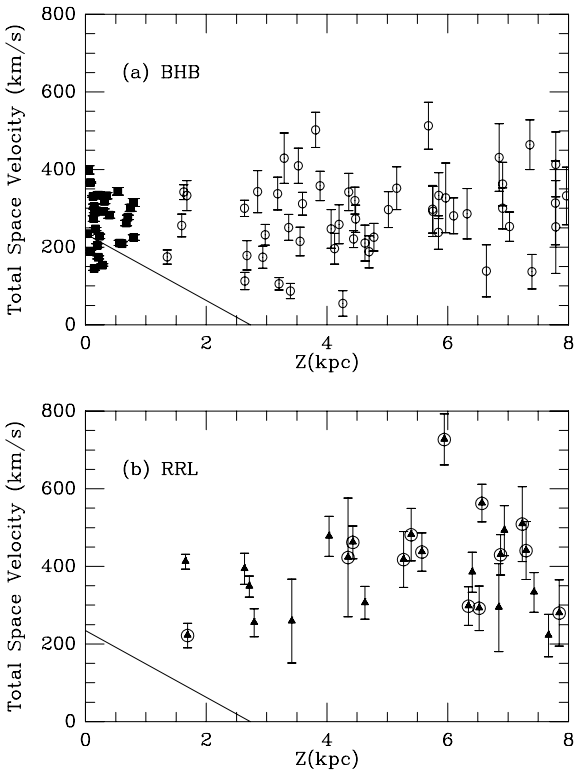

Figure 6. Plots of the total space velocity (T) in km s^{-1} as a function of the distance from the galactic plane (Z) in kpc for (a) BHB stars and (b) RRL stars. The BHB stars at the NGP are shown by open circles and local BHB stars by filled squares. The RRL stars are shown by filled triangles; those with W-velocities <-50 km s^{-1} are shown by encircled triangles. All stars above the line would be classified as belonging to the HALO2 sample of Martin & Morrison (1998).

of T that are well below the Galactic escape velocity of from 500 to 600 km s^{-1} (Smith et al. 2006). Possible exceptions are CK COM and SA57-47 that have $T=563\pm49$ and 727 ± 66 km s^{-1}, respectively. Large total space motions are associated with (i) stars with $4<Z<8$ kpc; (ii) RRL stars rather than BHB stars; (iii) RRL stars with large negative W velocities and (iv) RRL stars whose periods

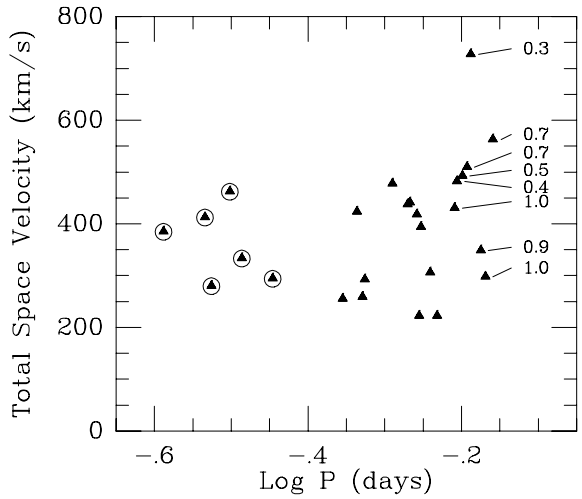

Figure 7. The total space velocity (T) in km s^{-1} for the RRL stars with Z<8 kpc plotted against the logarithm of the period P (d). The encircled triangles are of type c. A period of 0.60 d corresponds to $\log P = -0.221$. The numbers by the symbols representing the longer period variables are their visual amplitudes.

are greater than 0.60 d (Fig. 7 and Table 11). Among the longer period RRL stars, the ones with lower amplitudes have the larger T (Fig. 7). For periods greater than 0.60 d, we would expect those of lower amplitude to belong to Oosterhoff Class I and the higher amplitude variables to belong to Oosterhoff Class II. The mean period $\langle P_{ab}\rangle$ of the 20 type *ab* RRL that have $Z < 8$ kpc is 0.57 d. Our assumed RRL absolute magnitudes are linked to the RRL in the LMC whose $\langle P_{ab}\rangle$ are 0.583 and 0.573 d from the massive compact halo objects program (MACHO) (Alcock et al. 1996) and optical gravitational lensing experiment (OGLE) (Soszyński et al. 2003) surveys, respectively. The $\langle P_{ab}\rangle$ of the RRL stars in Galactic globular clusters is 0.585 d (Clement et al. 2001); 65 per cent of these variables are Oosterhoff type I.[8] This suggests that the LMC contains predominantly Oosterhoff type I variables. This is confirmed by their Fourier types (Alcock et al. 2004), and so our distances should be correct for Oosterhoff I variables which (judging from their $\langle P_{ab}\rangle$) probably comprise most of our sample. If, however, the Oosterhoff II variables are as much as ∼0.2 mag brighter than the Oosterhoff I variables (Lee and Carney 1999), then their distances and their total space velocities will have been underestimated. This may explain some of the dispersion in T for the RRL stars with $P > 0.60$ d.

3.5 The Galactocentric space motions

The Galactocentric space motions of our program stars in the cylindrical vectors $\boldsymbol{V}_R, \boldsymbol{V}_\phi$ and $\boldsymbol{V}_z$ have been calculated according to the equations given by Kepley et al. (2006) which were chosen to be compatible with those used by Helmi et al. (1999). These velocities are given in Columns 7, 8 and 9, respectively, of Tables 8 and 9. The Z-coordinate in this galactocentric system is in the opposite direction to that in our heliocentric system so that the galactocentric V_z has the opposite sign to W in the heliocentric system. Galactocentric V_ϕ and heliocentric V are, respectively, negative and increasingly negative for *retrograde* orbits. The *mean* values of these space velocities $\langle V_R\rangle, \langle V_\phi\rangle$ and $\langle V_z\rangle$ for the program stars with $Z < 8$ kpc and their corresponding dispersions (after correction as described in Section 3.1) are given in Table 12. It is seen that the BHB stars show no galactocentric rotation $\langle V_\phi\rangle = -005 \pm 015$ km s^{-1} in agreement with the analysis of the RV of 1170 BHB stars from the SDSS by Sirko et al. (2004b). Table 12 also gives the dispersions in cylindrical coordinates derived by Sirko et al. for three of their samples which we call SDSS(a), SDSS(b) and SDSS(c). These refer to their whole sample, stars with $g < 18$ and stars with $g < 16$, respectively. The dispersions for our BHB are similar to those found for the BHB samples of Sirko et al. (2004b) and have $\sigma_R \sim \sigma_\phi$, whereas non-BHB samples of the local halo ellipsoid (Sirko et al. 2004b, table 1) are like our RRL sample and have $\sigma_R > \sigma_\phi$. There are only six RRL stars in our sample with positive V_ϕ compared to 20 with negative velocities; the corresponding numbers for the BHB sample are 25 and 27. A Fisher's 2 × 2 test shows that this difference is significant at the 96 per cent level. A Shapiro–Wilks test of the V_ϕ-distribution of the RRL stars shows no significant departure from normality. It therefore seems unlikely that the retrograde $\langle V_\phi\rangle$ of these stars is caused by the inclusion of a few RRL stars with highly retrograde orbits but rather is a property of the whole sample.

3.6 Stars with $Z > 8$ kpc

In this paper, we have chosen not to analyse the data for the 39 stars with $Z > 8$ kpc. At 10 kpc, the random errors in the proper motions produce errors in the space motions that are comparable with the space motions themselves, and the estimated 2σ systematic error will be ∼40 km s^{-1}. Currently, we do not have RV for all these fainter stars, and those whose velocities have errors $\geqslant$25 km s^{-1} should be re-observed.

4 SUMMARY AND CONCLUSIONS

The kinematics of the BHB and RRL stars in the NGP show that this halo sample is not homogeneous. The BHB stars show essentially no galactic rotation in agreement with Sirko et al. (2004b) while the RRL stars show a definite retrograde rotation. Our whole sample of 117 stars includes stars out to 16 kpc, but we restricted our discussion to the 52 BHB stars and 26 RRL stars with $Z < 8$ kpc whose space motions are the more reliable. This sample of 78 stars has a heliocentric $\langle V\rangle = -268 \pm 14$ which is in reasonable agreement with the retrograde rotation of −55 km s^{-1} found by Majewski (1992) and MMH for their SA57 sample of subdwarfs at a similar $\langle Z\rangle$. Both our BHB and RRL sample and their subdwarf sample show qualitatively similar dependencies of $U_{\rm hel}$ on $W_{\rm hel}$ and an excess of stars with negative $W_{\rm hel}$ (Fig. 4). We also find that our BHB stars with $Z <$ 8 kpc ($\langle Z\rangle = 4.7$ kpc) have $\sigma_r = 101 \pm 10, \sigma_\phi = 93 \pm 09$ and $\sigma_z =$ 81 ± 08. These dispersions are similar to those of the BHB sample of Sirko et al. (2004b) with $g \leqslant 18$ which has $\sigma_r = 97 \pm 10, \sigma_\phi =$ 109 ± 18 and $\sigma_z = 101 \pm 6$. These dispersions are more isotropic than local samples of halo stars that typically have $\sigma_r > \sigma_\phi > \sigma_z$. Qualitatively, this is what we might expect from a halo that is more flattened towards the plane and more spherical away from the plane and at greater galactocentric distances (Kinman, Wirtanen & Janes 1965; Wesselink 1987; Preston, Shectman & Beers 1991; Vivas & Zinn 2006). The local BHB sample (Local A in Table 10) has $\sigma_r =$ $129 \pm 18, \sigma_\phi = 80 \pm 11$ and $\sigma_z = 101 \pm 14$ so that $\sigma_R > \sigma_\phi$ but (unusually) also has $\sigma_z > \sigma_\phi$. Many of the stars in this sample were selected as early-type high-velocity stars by Stetson (1991) and so Local A may have some kinematic bias.

[8] The RRL stars in most of the intrinsically faint, metal-poor dSph galaxies have $\langle P_{ab}\rangle \geqslant 0.60$ d; the Sgr dSph, on the other hand, has $\langle P_{ab}\rangle = 0.574$ d (Cseresnjes 2003).

Table 12. Mean galactocentric space velocities V_R, V_ϕ and V_z (km s^{-1}) and their corrected dispersions σ_R, σ_ϕ and σ_z for our program BHB and RRL stars and for comparison the SDSS BHB stars of Sirko et al. (2004b) (a) whole sample, (b) with $g < 18$ and (c) with $g < 16$.

Star type	n	$\langle V_R \rangle$	σ_R	$\langle V_\phi \rangle$	σ_ϕ	$\langle V_z \rangle$	σ_z
(1)	(2)	(3)	(4)	(5)	(6)	(7)	(8)
RRL	26	-11 ± 35	162 ± 23	-095 ± 29	122 ± 17	$+043 \pm 17$	079 ± 11
BHB	52	-20 ± 16	101 ± 10	-005 ± 15	93 ± 9	$+005 \pm 12$	081 ± 08
All	78	-17 ± 15	124 ± 10	-035 ± 14	111 ± 9	$+017 \pm 10$	081 ± 09
SDSS(a)	1170	···	94 ± 08	···	098 ± 18	···	098 ± 05
SDSS(b)	773	···	97 ± 10	···	109 ± 18	···	101 ± 06
SDSS(c)	227	···	109 ± 20	···	122 ± 24	···	094 ± 12

Our RRL stars that have positive *W*-velocities not only have a much smaller velocity dispersion (σ_v) than those with negative *W*-velocity, but also have the ratio of RRL to BHB stars significantly lower in this group compared with the group that has negative *W*-velocities. This inhomogeneity therefore involves a streaming motion that covers a significant part of our survey area and which is more pronounced for the stars with an RA $> 13^h00$. A similar streaming occurs in the subdwarf sample of MMH in the same part of the sky. A model of the Sgr stream (fig. 1 of Martínez-Delgardo et al. 2006) also predicts an infall in the Northern Galactic Cap but not quite in the direction of our survey, and probably refers to more distant stars than most of those in our sample. The streaming that we have observed may be connected with the Virgo overdensity (Lupton et al. 2005) but this overdensity is not yet sufficiently well defined for this to be more than a speculation.

The simultaneous use of *two* halo tracers (BHB and RRL stars) has shown that the halo has two field star components that seem to parallel the old and young components of the halo globular clusters. This is not at all a new idea. Thus, Wilhelm et al. (1996) (who give references to previous suggestions for two-component haloes) analysed the RV of 525 BHB stars and found an 'inner' flattened halo ($Z < 4$ kpc) in prograde ($+40 \pm 17$ km s^{-1}) rotation and an 'outer' ($Z > 4$ kpc) more spherical halo with a retrograde (-93 ± 36 km s^{-1}) rotation . This relatively high retrograde motion for the 'outer' BHB stars does not agree with either our results or those of Sirko et al. (2004b). A $Z > 4$ kpc sample will be at high galactic latitudes where the stars lie far from the apices of galactic rotation and their RV are relatively insensitive to the galactic rotation vector. This insensitivity of the RV and also possible inhomogeneities in the halo may be responsible for this discrepancy. On the other hand, the analysis of the space motions of halo stars by Chiba & Beers (2000) found no evidence for a retrograde 'high halo', possibly because their sample did not extend far enough from the solar neighbourhood.

The two halo components that fit our data are similar to those discussed by Borkova & Marsakov (2003) from their analysis of the space motions of nearby RRL stars. One component is associated with a strong BHB, has no galactic rotation and has a relatively isotropic velocity dispersion. The other component is characterized by having RRL stars whose $\langle P_{ab} \rangle$ shows that they are mostly of Oosterhoff type I. This second component has, on average, a retrograde rotation and a less isotropic velocity dispersion than the first component. Our second component also has streaming in its *W* space motion which suggests that it consists of tidal debris. This does not mean that the first component contains no RRL stars or the second has no BHB stars but that the BHB stars predominate in the first component and the RRL stars in the second. We would expect that the first component, having a BHB, would be associated with Oosterhoff type II RRL stars. We must be careful about this assertion, however, because there is considerable scatter in the HB-type versus $\langle P_{ab} \rangle$ plot; e.g. M62 has $\langle P_{ab} \rangle = 0.548$ d (Oosterhoff type I) and yet has a blue-HB (Clement et al. 2001; Conteras et al. 2005).

It would be quite desirable to be able to compare all the properties ([Fe/H], space densities, HB type, Oosterhoff type, etc.) of the halo stars in the North Polar Cap with those in the solar neighbourhood. This is beyond the scope of this paper and would require considerable attention to selection effects. As an example, all RRL surveys miss variables with amplitudes below a certain limit. Our photometry of the BHB stars showed that a number of these were low-amplitude RRL stars so, in this respect, our polar sample is unusually complete and contains low-amplitude long-period type-*ab* and -*c* variables that were missed in earlier surveys. Our results do not necessarily conflict with those of earlier surveys that have sampled larger volumes of space. The volume of space that we have sampled is relatively small. At the mean distance of 5 kpc, the width of the field is no more than $\sim$1 kpc. This may account for the pronounced lack of uniformity of the halo that we have found at the NGP and makes it essential that similar surveys should be made at other key locations such as the South Galactic Pole and the Anti-centre, and if possible that they should include more than one halo tracer.

ACKNOWLEDGMENTS

We thank D.R. Soderblom for kindly making available the program to calculate the *UVW* space motions. We are also grateful to Dr C. Clement for helpful comments on fundamentalizing RRL periods and A. Sollima for assistance in providing us with the infrared ZAHBs. This research has made use of 2MASS data provided by the NASA/IPAC Infrared Science Archive, which is operated by the Jet Propulsion Laboratory, California Institute of Technology, under contract with the National Aeronautics and Space Administration.

The GSC-II is a joint project of the Space Telescope Science Institute (STScI) and the INAF-Osservatorio Astronomico di Torino (INAF-OATo). We acknowledge the GSC-II team and in particular M.G. Lattanzi, B. McClean and R.L. Smart for their valuable support to this study.

This work is partly based on observations made with the Italian Telescopio Nazionale Galileo operated on the island of La Palma by the Fundacion Galileo Galilei of the INAF (Istituto Nazionale di Astrofisica) at the Spanish Observatorio del Roque de los

Muchachos of the Instituto de Astrofisica de Canarias and PRIN INAF 2005 1060803.

This research has made use of the SIMBAD database, operated at CDS, strasbourg, France.

This work has been partly supported by the MIUR (Ministero dell'Istruzione, dell'Università e della Ricerca) under PRIN-2001-1028897 and PRIN-2005-1060802.

REFERENCES

Alcock C., Allsman R., Axelrod T., Bennett D. et al., 1996, AJ, 111, 1146
Alcock C., Alves D., Axelrod T., Becker T. et al., 2004, AJ, 127, 334
Altmann M., Catelan M., Zoccali M., 2005, A&A, 439, 5
Battaglia G., Helmi A., Morrison H. et al., 2005, MNRAS, 364, 433
Beers T. C., Wilhelm R., Dionidis S. P., Mattson C. J., 1996, ApJS, 103, 433
Beers T. C., Chiba M., Yoshii Y., Platais I., Hanson R. B., Fuchs B., Rossi S., 2000, AJ, 119, 2866
Belokurov V., Zucker D., Evans N., Gilmore G. et al., 2006, ApJ, 642, L137
Bessell M., Castelli F., Plez B., 1998, A&A, 333, 231
Borkova T., Marsakov V., 2003, A&A, 398, 133
Brown W. R., Allende Prieto C., Beers T. C., Wilhelm R., Geller M. J., Kenyon S. J., Kurtz M. J., 2003, AJ, 126, 1362
Brown W. R., Geller M. J., Kenyon S. J., Beers T. C., Kurtz M. J., Roll J. B., 2004, AJ, 127, 1555
Brown W. R., Geller M. J., Kenyon S. J., Kurtz M. J., Allende Prieto C., Beers T. C., Wilhelm R., 2005, AJ, 130, 1097
Cardelli J. A., Clayton G. C., Mathis J. S., 1989, ApJ, 345, 245
Carney B. W., 1999, in Gibson B. K., Axelrod T. S., Putman M. E., eds, ASP Conf. Ser. Vol. 165, The Third Stromlo Symposium: The Galactic Halo. Astron. Soc. Pac., San Francisco, p. 230
Chiba M., Beers T. C., 2000, AJ, 119, 2843
Chiba M., Mizutani A., 2004, Publ. Astron. Soc. Aust., 21, 237
Christlieb N., Beers T., Thom C., 2005, A&A, 431, 143
Clement C., Muzzin A., Dufton Q. et al., 2001 AJ, 122, 2587
Clementini G., Gratton R., Bragaglia A., Carretta E., Di Fabrizio L., Maio M., 2003, AJ, 125, 1309
Clewley L., Warren S. J., Hewett P. C., Norris J. E., Peterson R. C., Evans N. W., 2002, MNRAS, 337, 87
Clewley L., Warren S. J., Hewett P. C., Norris J. E., Evans N. W., 2004, MNRAS, 352, 285
Clewley L., Warren S. J., Hewett P. C., Norris J. E., Wilkinson M. I., Evans N. W., 2005, MNRAS, 362, 349
Clewley L., Kinman T. D., 2006, MNRAS, 371, L11
Conteras R., Catelan M., Smith H. A., Pritzl B. J., Borissova J., 2005, ApJ, 623, 117
Cseresnjes P., 2003, A&A, 375, 909
De Angeli F., Piotto G., Cassisi S., Busso G., Recio-Blanco A., Salaris M., Aparicio A., Rosenberg A., 2005, AJ, 130, 116
Dehnen W., Binney J. J., 1998, MNRAS, 298, 387
Duffau S., Zinn R., Vivas A. K., Carraro G., Méndez R. A., Winnick R., Gallart C., 2006, ApJ, 636, L97
Ferraro F. R., Carretta E., Corsi C. E., Fusi Pecci F., Cacciari C., Buonanno R., Paltrinieri B., Hamilton D., 1997, A&A, 320, 757
Freedman W. L. et al., 2001, ApJ, 553, 47
GAIA Concept and Technology Study Report 2004, ESA-SCI(2004)4
Gilmore G., Wyse R. F. G., Norris J. E., 2002, ApJ, 574, L39
Helmi A., White S. D., de Zeeuw P. T., Zhao H., 1999, Nat, 402, 53
Harding P., Morrison H. L., Olszewski E. W., Arabadjis J., Mateo M., Dohm-Palmer R. C., Freeman K. C., Norris J. E., 2001, AJ, 122, 1397
Hewitt A., Burbidge G., 1993, ApJS, 87, 451
Ibata R., Gilmore G., Irwin M., 1994, Nat, 370, 194
Ibata R., Lewis G. F., Irwin M., Totten E. J., Quinn T., 2001, ApJ, 551, 294
Ivezić Z., Goldston J., Findlator K. et al., 2000, AJ, 120, 963
Johnson D. R. H., Soderblom D. R., 1987, AJ, 93, 864
Jones B. F., Walker M. F., 1988, AJ, 95, 1755
Jones R. V., Carney B. W., Fulbright J. P., 1996, PASP, 108, 877
Jurić M., Ivezić Z., Brooks A. et al., 2006, ApJ, submitted (astro-ph/0510520)
Kepley A., Morrison H., Helmi A., Kinman T. et al. 2006, AJ, submitted
Kholopov P. N., Samus N. N., Kazarovets E. V., Perova N. B., 1985, Inf. Bull. Var. Stars, 5311
Kinman T. D., Wirtanen C. A., Janes K. A., 1965, ApJS, 11, 223
Kinman T. D., Suntzeff N. B., Kraft R. P., 1994, AJ, 108, 1722
Kinman T. D., Pier J. R., Suntzeff N. B., Harmer D. L., Valdes F., Hanson R. B., Klemola A. R., Kraft R. P., 1996, AJ, 111, 1164
Kinman T. D., Castelli F., Cacciari C., Bragaglia A., Harmer D., Valdes F., 2000, A&A, 364, 102
Kinman T. D., 2002, Inf. Bull. Var. Stars, 5311
Kinman T. D., Cacciari C., Bragaglia A., Buzzoni A., Spagna A., 2003, in Boily C. M., Patsis P., Portegies-Zwart S., Spurzem R., Theis C., eds, Galactic, Stellar Dynamics. Proceedings of JENAM 2002, EAS Pub. Ser., Vol. 10, EDP Sciences, Les Ulis, p. 115
Kinman T. D., Bragaglia Cacciari, C.A., Buzzoni A., Spagna A., 2005, The Three-Dimensional Universe with GAIA. ESA SP-576, ESA, Noordwijk, p. 175
Lasker B. M., McLean B. J., Jenkner H., Lattanzi M. G., Spagna A., 1995, in Perryman M. A. C., van Leeuwen F., Guyenne T. D., eds, Future Possibilities for Astrometry in Space. ESA SP-379, ESA, Noordwijk, p. 137
Law D. R., Johnson K. V., Majewski S., 2005, ApJ, 619, 807
Layden A., 1996, in Morrison H., Sarajedini A., eds, ASP Conf. Ser. Vol. 92, The Formation of the Galactic Halo: Inside and out. Astron. Soc. Pac., San Francisco, p. 141
Lee J., Carney B. W., 1999, AJ, 118, 1373
Lupton R., Juric M., Ivezic Z., Brooks A. et al., 2005, BAAS, 37, 1384
MacConnell D. J., Stephenson C. B., Pesch P., 1993, ApJS, 86, 453
Maintz G., de Boer K. S., 2005, A&A, 442, 229
Majewski S. R., 1992, ApJS, 78, 87
Majewski S., Munn J. A., Hawley S. L., 1996, ApJ, 459, L73 (MMH)
Majewski S. R., Skrutskie M. F., Weinberg M. D., Ostheimer J. C., 2003, ApJ, 599, 1082
Martin J. C., Morrison H. L., 1998, AJ, 116, 1724
Martínez-Delgardo D., Peñarrubia J., Juric M., Alfaro E. J., Ivezic Z., 2006, preprint (astro-ph/0609104)
McLean B. J., Greene G. R., Lattanzi M. G., Pirenne B., 2000, in Manset N., Veillet C., Crabtree D., eds, ASP Conf. Ser. Vol. 216, ADASS IX. Astron. Soc. Pac., San Francisco, p. 145
Meza A., Navarro J. F., Abadi M. G., Steinmetz M., 2005, MNRAS, 359, 93
Monaco L., Bellazzini M., Ferraro F. R., Pancino E., 2003, ApJ, 597, L25
Morrison H. L., Mateo M., Olszewski E. W., Harding P., Dohm-Palmer R. C., Freeman K. C., Norris J. E., Morita M., 2000, AJ, 119, 2254
Nemec J. M., Linnell-Nemec A. F., Lutz T. E., 1994, AJ, 108, 222
Newberg H. J., Yanny B., Rockosi C. et al., 2002, ApJ, 569, 245
Paltrinieri B., Ferraro F. R., Fusi Pecci F., Carretta E., 1998, MNRAS, 293, 434
Preston G. W., Shectman S. A., Beers T. C., 1991, ApJ, 375, 121
Rosenberg A., Saviane I., Piotto G., Aparicio A., 1999, AJ, 118, 2306
Sandage A., 2006, AJ, 131, 1750
Sanduleak N., 1988, ApJS, 66, 309
Schlegel D. J., Finkbeiner D. P., Davis M., 1998, ApJ, 500, 525
Shapiro S. S., Wilk M. B., 1965, Biometrika, 52, 591
Sirko E., Goodman J., Knapp G. R. et al., 2004a, AJ, 127, 899
Sirko E., Goodman J., Knapp G. R. et al., 2004b, AJ, 127, 914
Smith M., Ruchti G., Helmi A., Wyse R. et al., 2006, preprint (astro-ph/0611671)
Soszyński I., Udalski A., Symański M. et al., 2003, Acta Astron., 53, 93
Spagna A., Lattanzi M. G., Lasker B. M., McLean B. J., Massone G., Lanteri L., 1996, A&A, 311, 758
Stetson P., 1991, AJ, 102, 589
Takase B., Miyauchi-Isobe N., 1993, Publ. Natl. Astron. Obs. Japan, 3, 169
Tammann G. A., Sandage A., Reindl B., 2003, A&A, 404, 423
Thom C., Flynn C., Bessell M. S. et al., 2005, MNRAS, 360, 354
Totten E. J., Irwin M. J., 1998, MNRAS, 294, 1
Totten E. J., Irwin M. J., Whitelock P. A., 2000, MNRAS, 314, 630
Valenti E., Ferraro F. R., Perina S., Origlia L., 2004, A&A, 419, 139
Vallenari A., Pasetto S., Bertelli G., Chiosi C., Spagna A., Lattanzi M., 2006, A&A, 451, 125

van den Bergh S., 1993, AJ, 105, 971
Vandenberg D. A., Swenson F. J., Rogers F. J., Iglesias C. A., Alexander D. R., 2000, ApJ, 532, 430
Véron-Cetty M., Véron P., 2001, CDS VizieR (VII/224)
Vivas A. K., Zinn R., Andrews P. et al., 2001, ApJ, 554, L33
Vivas A. K., Zinn R., 2006, AJ, 132, 714
Wesselink Th., 1987, PhD thesis. Catholic University of Nijmegen, The Netherlands
Wilhelm R., Beers T., Kriessler J. et al., 1996, in Morrison H., Sarajedini A., eds, ASP Conf. Ser. Vol. 92, The Formation of the Galactic Halo: Inside and Out. Astron. Soc. Pac., San Francisco, p. 171
Yanny B., Newberg H. J., Kent S. et al., 2000, ApJ, 540, 825
Zacharias N., Monet D. G., Levine S. E., Urban S. E., Gaume R., Wycoff G. L., 2004, BAAS, 36, 1418
Zinn R., 1993, in Smith G., Brodie J., eds, ASP Conf. Ser. Vol. 48, The Globular Cluster–Galaxy Connection. Astron. Soc. Pac, San Francisco, p. 38

This paper has been typeset from a TEX/LATEX file prepared by the author.